

A new methodology for performing large scale simulations of tsunami generated by deformable submarine slides

Rebecca C. Smith^{a,1,*}, Jon Hill^b, Simon L. Mouradian^a, Matthew D. Piggott^a,
Gareth S. Collins^a

^a*Department of Earth Science and Engineering, Imperial College London, SW7 2AZ, UK.*

^b*Department of Geography and Environment, University of York, Heslington, York, YO10 5DD, UK*

Abstract

Large tsunamis can be generated by submarine slides, but these events are rare on human timescales and challenging to observe. Experiments and numerical modelling offer methods to understand the mechanisms by which they generate waves and what the potential hazard might be. However, to fully capture the complex waveform generated by a submarine slide, the slide dynamics must also be accurately modelled. It is computationally difficult to model both a three-dimensional submarine slide whilst simultaneously simulating oceanic-scale tsunamis. Past studies have either coupled localised models of the slide generation to oceanic-scale tsunami simulations or simplified the slide dynamics. Here, we present a new methodology of model coupling that generates the wave in the ocean-scale model via boundary-condition coupling of a two-dimensional dynamic slide simulation. We verify our coupling methodology by comparing model results to a previous simulation of a tsunamigenic slide in the Gulf of Mexico. We then examine the effect of slide deformation on the risk posed by hypothetical submarine slides around the UK. We show the deformable

*Corresponding author

Email address: `rebecca.smith08@alumni.imperial.ac.uk` (Rebecca C. Smith)

¹Present Address: Risk Management Solutions, 30 Monument Street, London, EC3R 8NB, UK

submarine slide simulations produce larger waves than the solid slide simulations due to the details of acceleration and velocity of the slide, although lateral spreading is not modelled. This work offers a new methodology for simulating oceanic-scale tsunamis caused by submarine slides using the output of a two-dimensional, multi-material simulation as input into a three-dimensional ocean model. This facilitates future exploration of the tsunami risk posed by tsunamigenic submarine slides that affect coastlines not normally prone to tsunamis.

Keywords:

Submarine Slide, Tsunami, Numerical Modelling, Landslides,

1. Introduction

Tsunamigenic submarine slides are rare on human timescales and are difficult to monitor or directly observe because it is not possible to predict their occurrence. Therefore, experiments and numerical modelling are important for understanding the submarine slide dynamics, failure, tsunamigenic potential, and forecasting the characteristics of the generated tsunami (Masson et al., 2006; Harbitz et al., 2014). Laboratory experiments are useful to approximate natural conditions with typical materials, however numerical modelling is the only way to simulate events at real scale and with complete and complex geometry and bathymetry (Bornhold and Thomson, 2012). This is essential to assess the potential hazard posed by such events.

The passive Atlantic margin is the source of a number of geologically recent submarine slides, the largest of which was the Storegga Slide, which occurred offshore Norway approximately 8.2 ka (Bugge et al., 1988; Dawson et al., 1988; Smith et al., 2004; Bondevik et al., 2005a; Wagner et al., 2007) with an estimated slide volume of 2400–3200 km³ (De Blasio et al., 2005). Deposits from the resulting tsunami indicate vertical run-ups of over 20 m on the Shetlands Islands and Norwegian coast

17 (Bondevik et al., 2005a,b; Dawson et al., 1988; Smith et al., 2004; Wagner et al.,
18 2007). Storegga is the most recent of a series of large submarine slides that have
19 occurred in this area of the Nordic Seas throughout geological history (Laberg et al.,
20 2002a,b; Bryn et al., 2003; Solheim et al., 2005). There is some debate over the
21 recurrence interval, however, the most recent studies suggest six very large slides
22 occurred in the last 20 ka, which indicates a recurrence interval of 3–4 ka for the area
23 (Talling, 2013). Furthermore, not all slides on the Norwegian and UK margins may
24 have also initiated tsunami, depending on the size, depth, speed and acceleration of
25 slide blocks.

26 Studies of submarine slide tsunami often break the process down into four parts:
27 1) the dynamics of the submarine slide, 2) the wave generation, 3) the wave propaga-
28 tion and 4) the tsunami wave inundation/run-up at coastlines. Numerical modelling
29 of large-scale submarine slide generated tsunami from the initiation of submarine
30 slide motion and wave generation, through to wave propagation and inundation in
31 three dimensions, is computationally challenging, owing to the large slide dimensions
32 and long run-out distances. Furthermore, within the large computational domains
33 required, many aspects must be modelled at high resolution, such as the slide mo-
34 tion and the coastlines. Therefore, numerical simulations have tended to rely on
35 simplifications to make the problem more tractable.

36 Many studies have simplified steps (1)–(3) by modelling the slide as a rigid block
37 with prescribed motion, and employing the shallow-water approximation (e.g. Har-
38 bitz 1992; Ma et al. 2012 and Hill et al. 2014). However, rigid block models do not
39 account for deformation of the slide and incorporate profiles for slide velocity and
40 acceleration that must be estimated. Since several studies have shown that sub-
41 marine slide acceleration and velocity are key parameters in determining resulting
42 wave characteristics (Harbitz, 1992; Harbitz et al., 2014; Løvholt et al., 2015), this

43 suggests that accurate representation of the slide dynamics is imperative to achieve
44 accurate wave heights in simulations. The shallow water (long-wave) approximation
45 relies on the assumption that the horizontal scale of the wave motion is consid-
46 erably larger than the local water depth or vertical scale (Harbitz, 1992; Jiang and
47 LeBlond, 1992, 1993; Thomson et al., 2001; Fine et al., 1998, 2005; Assier-Radkiewicz
48 et al., 2000; Yavari-Ramshe and Ataie-Ashtiani, 2015). Shallow water models become
49 increasingly less appropriate in increasing water depths and decreasing water wave-
50 lengths, as dispersion becomes more important (Bornhold and Thomson, 2012) and
51 this approximation neglects frequency dispersion and vertical velocity/acceleration.
52 Whilst this approximation is generally appropriate for seismogenic tsunami, it may
53 not be appropriate for submarine slide generated waves, which often have shorter
54 wavelengths (Glimsdal et al., 2013; Løvholt et al., 2015).

55 Some numerical studies have modelled deformation of submarine slides. In order
56 to model the slide deformation, many of these studies are restricted in terms of
57 domain size, scale or consider an approximation to the full Navier–Stokes equations.
58 Studies that model the slide as a Newtonian, viscous fluid but were restricted to
59 lab scale are Assier-Rzadkiewicz et al. (1997) and Abadie et al. (2010). Fine et al.
60 (2005) and Assier-Radkiewicz et al. (2000) employ similar slide models but rely on
61 the shallow water approximation in order to model a full-scale slide. Some studies
62 have also used a Bingham rheology for the slide, a non-Newtonian fluid where the
63 deformation is dependant on stress. Examples of this at the laboratory scale include
64 Assier-Rzadkiewicz et al. (1997) and Gauer et al. (2005). Jiang and LeBlond (1993)
65 and Gauer et al. (2006) use a similar rheological model over a large domain, but
66 applying the shallow water approximation. Ma et al. (2013) modelled the slides as
67 a water–sediment mixture and Capone et al. (2010), Ataie-Ashtiani and Shobeyri
68 (2008) and Snelling et al. (2020) used Smoothed Particle Hydrodynamics (SPH) to

69 recreate laboratory experiments. Lee and Huang (2018) and Yu and Lee (2019) used
70 a multi-phase flow model to simulate underwater landslides and wave generation.
71 Many of the domains considered in these studies are restricted to a small area due to
72 the high-resolution required to capture the dynamics of the slide. In order to simulate
73 the tsunami propagation a second model has to be coupled to the slide model or the
74 spatial resolution is too low to capture detailed dynamics in the waveform generated
75 by the slide motion.

76 In reality, submarine slides deform with complex rheology and flow (Grilli and
77 Watts, 2005; Løvholt et al., 2015). Simulating the slide dynamically, including its
78 interaction with the water, internal deformation and drag, ensures a more accurate
79 description of slide acceleration and velocity, but adds substantial complexity and
80 computational expense. The importance of realistic slide dynamics (i.e. acceleration
81 and maximum velocity) and internal deformation during the wave-generating stage of
82 slide motion motivates the choices of numerical modelling approach used in this work.
83 While approximations to the full Navier-Stokes equations are often valid, in order
84 to investigate fully the effects and importance of slide dynamics and deformability
85 on wave generation, the use of full Navier-Stokes models allows vertical acceleration
86 to be considered and provides a more complete representation than shallow water
87 models, particularly for relatively small slides (Watts et al., 2003; Abadie et al., 2012;
88 Glimsdal et al., 2013; Horrillo et al., 2013).

89 Fluidity is a computational fluid dynamics framework that allows for the nu-
90 merical solution of several equation sets in three dimensions (Piggott et al., 2008;
91 AMCG, 2014). Fluidity has previously been used in two dimensions to model de-
92 formable submarine slides and accurately represent slide, water (and air) to simulate
93 the generation of tsunami waves (Smith et al., 2016). The approaches in Smith et al.
94 (2016) explicitly modelled the submarine slides (as Newtonian viscous fluids) and

95 therefore helped to improve understanding of the submarine slide failure process and
96 the forces that act upon the slide and water. However, the methods are computation-
97 ally expensive to run owing to the modelling of multiple materials and requirement
98 of high resolution meshes to resolve the complex and small-scale slide dynamics and
99 the coupling to wave generation. The application of mesh adaptivity was able to
100 reduce the computational expense, but the ability to apply this to much larger, and
101 three-dimensional, computational domains is still restricted. Therefore previous work
102 only considered two-dimensional, vertical slice domains over the tsunami generation
103 region (Smith et al., 2016). To fully quantify the importance of slide deformation
104 and dynamics for a hazard assessment, it is important to study wave generation and
105 propagation in three dimensions to allow consideration of geometric spreading, wave
106 interaction with the coastlines, the effect of the direction of slide failure and wave
107 inundation. Extending multi-material approaches to significantly larger domains,
108 whilst maintaining the high resolution and number of materials would require an
109 increase in computational cost that is not currently practical. Therefore other ap-
110 proaches that are less computationally demanding are required.

111 A new, computationally efficient approach for modelling submarine slide tsunami
112 is presented here that accounts for slide dynamics and deformation, and wave gener-
113 ation and propagation, in three dimensions using Fluidity (Piggott et al., 2008). The
114 motion of the submarine slide is incorporated via a prescribed boundary condition
115 applied on the sea floor of the computational domain (e.g. Hill et al. 2014). This
116 mimics the effect of the submarine slide motion on the water column and allows
117 the number of materials that are modelled to be reduced by omitting the submarine
118 slide and modelling only the water. Consequently, the requirement for high vertical
119 resolution is removed and thus computational expense is reduced significantly. As a
120 result, the model can be applied over an increased area, and in three dimensions, to

121 model the generation and propagation of the wave towards coastlines. This approach
122 is referred to as the Single Material (SM) method. Previously, such approaches have
123 assumed a rigid slide body (that cannot fully account for all the forces acting upon
124 a submarine slide that will in turn affect wave generation) and a simplified, idealised
125 acceleration and deceleration profile. This approach is similar to that used by Fine
126 et al. (2005), Ma et al. (2012) and Harbitz (1992) but is novel in that the full Navier-
127 Stokes equations are used instead of the shallow water approximation, and differs
128 from Harbitz (1992) where the free surface height is altered in the shallow water
129 equations. We use three different numerical approaches to model submarine slide
130 tsunami, within the same framework. This has allowed for comparison of approaches
131 without the complication of separate models and an understanding of the limitations
132 and advantages of each method. These three-dimensional modelling techniques are
133 then applied to advance understanding of the coastal hazard from submarine slide
134 tsunami.

135 *1.1. Outline*

136 In this work, the output (change in position and thickness of a slide) of a two-
137 material simulation (MM2FS, Smith et al. 2016), is extracted and used as a boundary
138 condition for the single-material (SM) simulation. The coupling of these models
139 forms an approach termed Single Material, Deformable Slide, Simulated Velocity
140 (SM-DS-SV). Another approach uses a rigid slide with a velocity profile (SM-RS-EV:
141 Single Material, Rigid Slide, Estimated Velocity) that is estimated using a simple
142 momentum balance on an inclined slope that is representative of the slope on which
143 the slides lies (Harbitz, 1992). A further approach assigns a velocity profile to the
144 rigid slide that is based on the motion of the centre of mass of the slide in an
145 MM2FS simulation. This is a ‘hybrid’ approach between a rigid slide with a synthetic,

146 estimated velocity profile (SM-RS-EV) and a simulation that attempts to account
147 for more realistic slide dynamics and deformation using information extracted from
148 simulations that model the slide as a fluid. This approach is termed Single Material,
149 Rigid Slide, Simulated Velocity (SM-RS-SV). By comparing the waves generated by
150 the SM-RS-SV approach with the SM-DS-SV approach, the effect and importance
151 of slide deformation for wave generation can be isolated from the importance of slide
152 velocity and acceleration. Waves produced by these three methods are also compared
153 to waves produced by a rigid slide of equal volume moving with a prescribed velocity
154 profile, using a method similar to Harbitz (1992); Ma et al. (2012); Hill et al. (2014).

155 These approaches are first applied to a hypothetical submarine slide scenario in
156 the Gulf of Mexico (first modelled in two and three dimensions in Horrillo et al. (2013)
157 and in two dimensions in Smith et al. (2016)) and is now extended to three dimensions
158 using Fluidity and the SM-RS-EV, SM-RS-SV and SM-DS-SV approaches to verify
159 correct implementation of the model. We then show the effect modelling deformation
160 of the tsunamigenic slide has on tsunami risk from two hypothetical slides offshore
161 of the UK.

162 **2. Methods**

163 *2.1. Fluidity*

Fluidity is an open source, general purpose, computational fluid dynamics, frame-
work (Piggott et al., 2008). The flexible finite-element/control-volume discretisation
approach, allows for the numerical solution of several equation sets (Piggott et al.,
2008). It has been used in a number of fluid flow studies, ranging from laboratory to
ocean-scale (e.g. Wells et al., 2010; Hill et al., 2012; Hiester et al., 2011; Parkinson
et al., 2014). In an ocean modelling context, Fluidity has been used to model both

modern and ancient earthquake-generated tsunami (Oishi et al., 2013; Mitchell et al., 2010; Shaw et al., 2008), and tsunami generated by three-dimensional rigid-block submarine slides with prescribed motion, in a study of the ancient Storegga Slide (Hill et al., 2014). Fluidity uses unstructured meshes, which can be multiscale but fixed, or fully dynamically adaptive. Multiscale meshes have spatially varying resolution, which can vary by orders of magnitude (Piggott et al., 2008). This enables complex coastlines and bathymetry to be accurately represented without “staircase” effects (Wells et al., 2005). The reduction in computational expense by using multiscale or adaptive meshes may allow for the simulation of wave generation and propagation of slides that are larger than it has previously been possible to model. Here, the non-hydrostatic incompressible Navier-Stokes equations under the Boussinesq approximation are solved in a rotating reference frame:

$$\frac{\partial \mathbf{u}}{\partial t} + \mathbf{u} \cdot \nabla \mathbf{u} + 2\boldsymbol{\Omega} \times \mathbf{u} = -\nabla \left(\frac{p}{\rho} \right) + \nabla \cdot (\boldsymbol{\nu} \nabla \mathbf{u}) - g\mathbf{k}, \quad (1a)$$

$$\nabla \cdot \mathbf{u} = 0, \quad (1b)$$

164 where \mathbf{u} is the 3D velocity vector, t represents time, p is pressure, $\boldsymbol{\nu}$ is the kinematic
 165 viscosity tensor and ρ denotes the density, which is constant in this work. $\boldsymbol{\Omega}$ is the
 166 rotational velocity of the Earth and g is the gravitational acceleration with \mathbf{k} pointing
 167 in the radial, upward direction. The seabed boundary condition is then dictated by
 168 the methodology used.

169 *2.2. MM2FS: Two-material model: viscous slide and water, with a free surface*

170 The MM2FS approach is one of a number of approaches for modelling submarine
 171 slide tsunami generation introduced in Smith et al. (2016). Two materials (slide and
 172 water) are modelled as viscous fluids and described using volume fraction fields with
 173 different densities and viscosities. The slide is simulated in two-dimensions along the
 174 vertical plane in which the slide travels.

175 For incompressible flows with variable density, as in the case of multiple materials,
 176 an additional equation is required to close the system, we refer to this as the equation
 177 of state. In the approach used here, this equation relates the bulk density to the
 178 volume fractions of materials in the problem, along with the associated material
 179 properties.

180 A volume fraction field, φ_i , is used to describe the location of different materials.
 181 In MM2FS $n_\varphi = 2$, φ_i varies in $[0, 1]$ and should sum to unity everywhere:

$$\sum_{i=1}^{n_\varphi} \varphi_i = 1. \quad (2)$$

182 Since, from (2), one of the volume fraction fields (here always water) can be
 183 recovered from the others using

$$\varphi_{n_\varphi} = 1 - \sum_{i=1}^{n_\varphi-1} \varphi_i, \quad (3)$$

184 $n_\varphi - 1$ advection equations of the form

$$\frac{\partial \varphi_i}{\partial t} + \mathbf{u} \cdot \nabla \varphi_i = 0, \quad (4)$$

185 need to be solved for the landslide.

186 In MM2FS, only one volume fraction is required, therefore only the landslide
 187 is tracked using Equation (4), while the location of the water is recovered using
 188 Equation (3). The bulk density and viscosity used in Equation (1a) is recovered
 189 from the volume fractions using:

$$\rho = \sum_{i=1}^{n_\varphi} \varphi_i \rho_i, \quad \mu = \sum_{i=1}^{n_\varphi} \varphi_i \mu_i, \quad (5)$$

190 where ρ_i and μ_i represent the constituent densities and viscosities of the individual
 191 materials. This method is similar to the VoF method used in TSUNAMI3D (Horrillo
 192 et al., 2013) and OpenFoam (Abadie et al., 2010). For more details of this model see
 193 Smith et al. (2016) and Smith (2017).

194 *2.3. SM: Single material and prescribed velocity boundary condition*

195 Submarine slide failure leads to water displacement. In this approach the total
196 water displacement is determined by the change in slide thickness along the ocean
197 floor caused by the slide movement. This water displacement is imposed as a normal
198 velocity Dirichlet boundary condition on the ocean floor, inducing a change in the
199 normal velocity, and is calculated as:

$$(\mathbf{u} \cdot \mathbf{n})^D = \frac{[h_s(x - x_s(t - \Delta t), y - y_s(t - \Delta t))] - [h_s(x - x_s(t), y - y_s(t))]}{\Delta t} \quad (6)$$

200 where Δt is the timestep of the model, and \mathbf{n} is the outward unit normal. The
201 parameters x_s and y_s are the horizontal coordinates and h_s is slide thickness. The
202 velocity vector is approximated using a linear discontinuous Galerkin approximation
203 (P1DG), whilst a quadratic continuous (P2) approximation is used for pressure.
204 Further details of the numerics may be found in Hill et al. (2014).

205 Fluidity is parallelised and this methodology is applied in all three single ma-
206 terial approaches (SM-RS-EV, SM-RS-SV and SM-DS-SV) irrespective of a solid
207 or deforming slide. Hill et al. (2014) tested Fluidity’s SM-RS-EV approach against
208 Haugen et al. (2005) in two dimensions and achieved good agreement between the
209 two models for a rigid slide. Three approaches to model the slide dynamics are
210 detailed below and summarised in Table 1.

211 *2.3.1. SM-DS-SV approach: Single material, deformable slide, simulated velocity*

212 The following work-flow is undertaken to move from two-dimensional multima-
213 terial, multilayer simulations to three-dimensional, single material, single layer sim-
214 ulations:

- 215 1. Run two-dimensional MM2FS simulation.

- 216 2. Extract from MM2FS the geometry/thickness and position of the slide, as a
217 function of distance, through time.
- 218 3. Use a low pass filter to smooth high-frequency fluctuations in the slide thickness
219 profile
- 220 4. Calculate the change in thickness of the slide, h_s , for every column of nodes in
221 the mesh. between the current timestep and the previous timestep to give a
222 velocity ($dv = dh/dt$)
- 223 5. Apply this velocity as boundary condition at the sea floor, in the local nor-
224 mal direction, in a simulation with reduced vertical resolution. The velocity
225 boundary condition is applied perpendicular to the slide transect, to a distance
226 of half the width of the slide either side.

227 Step (3) is required to remove any effect of the mesh on the shape of the submarine
228 slide by filtering out high-frequency fluctuations (discussed in Smith et al., 2016
229 and Horrillo et al., 2013). These fluctuations are caused by the sharp gradient in
230 density and velocity at the slide surface. The parameters of the low pass filter were
231 chosen so that the overall shape of the slide is preserved, but minor mesh-scale noise
232 (occurring on scales <100 m, the horizontal resolution of the MM2FS simulation)
233 in slide thickness is smoothed. This step ensures that when dh/dt is calculated
234 the mesh-scale changes are smoothed out and are negligible compared to the long
235 wavelength change in shape of the slide and does not result in ‘pulses’ in which could
236 lead to a ‘noisy’ boundary condition. Furthermore, the resolution in the slide region
237 of the SM–DS–SV simulation is coarser than the resolution in the MM2FS simulation
238 and therefore high frequency noise at this scale could not be accurately reproduced
239 on the coarser mesh.

240 *2.3.2. SM-RS-SV approach: Single material, rigid slide, simulated velocity*

- 241 1. Run two-dimensional MM2FS simulation.
- 242 2. Extract the displacement of the slide’s centre of mass from the MM2FS simu-
243 lation.
- 244 3. Calculate the velocity profile of the slide’s centre of mass using the displacement
245 extracted in (2) and the timestep.
- 246 4. Prescribe the motion of a rigid slide, with fixed and constant slide thickness
247 using a choice of one of these two velocities.

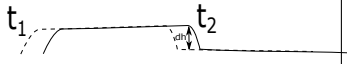
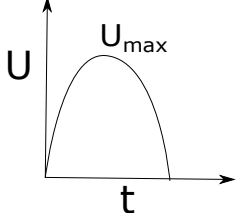
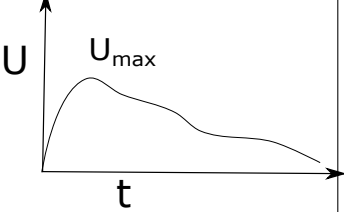
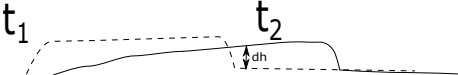
248 *2.3.3. SM-RS-EV approach: Single material, rigid slide, estimated velocity*

249 To estimate a velocity profile for the submarine slides in this work, a force balance
250 for a submerged submarine slide on a constant slope is used (Harbitz, 1992).

$$u_{term} = \sqrt{\frac{2(\rho_s - \rho_w)gh(\sin\alpha - \mu\cos\alpha)}{C_D\rho_w}}, \quad (7)$$

251 where ρ_s is the mean slide density, ρ_w is the density of the water surrounding the
252 slide, h is the average slide thickness, α is the slope angle, μ the coefficient of friction
253 between the slide and the seafloor, g the acceleration due to gravity and C_D is the
254 drag coefficient along the upper surface of the slide. Applying Equation (7) to the
255 Storegga Slide for reasonable values of μ and C_D , suggests $u_{term} = 56 \text{ ms}^{-1}$, however
256 studies show the maximum slide velocity that gives the best match to observed run-
257 up heights was about 60% of this, 35 ms^{-1} (Bondevik et al., 2005b; Hill et al., 2014).
258 Therefore the maximum velocity of the slides in this work is taken to be 60% of u_{term} .
259 The values for μ (0.005) and C_D (0.0025) are fixed and taken from Hill et al. (2014).
260 ρ_w and ρ_s are chosen to match the values in the MM2FS simulations (Smith et al.,
261 2016), 1000 kgm^{-3} and 2000 kgm^{-3} respectively. Therefore u_{max} is solely a function

Table 1: Comparison of SM-RS-EV, SM-RS-SV and SM-DS-SV approaches

	Vertical Velocity/ Shape Change	Horizontal Velocity/ Slide Velocity
SM-RS-EV Single Material, Rigid Slide, Estimated Velocity	 $v = \frac{dh}{dt} = \frac{(h_{t_1} - h_{t_2})}{(t_2 - t_1)}$ <p>For every node in the mesh in MM2FS</p>	
SM-RS-SV Single Material, Rigid Slide, Simulated Velocity	<p>As above</p>	 <p>where the velocity is the centre of mass of the slide from an MM2FS simulation</p>
SM-DS-SV Single Material, Deformable Slide, Simulated Velocity	 <p>Change in shape and location of slide extracted from MM2FS simulation</p>	

262 of the slide volume and the average slope, which is determined between the initial
 263 start and end depths of the slide. The velocity profile is chosen to be half-sinusoidal
 264 (in line with Harbitz (1992)), with the period $T = \frac{\pi}{2} \frac{R}{u_{max}}$, where R is the total run-
 265 out length, selected to be equal to the slide total length, $R = L + 2S$, where L is the
 266 ‘length’ of the slide, S the length over which the slide thickness tapers. The total
 267 run out distance consists of an acceleration phase, R_a and a deceleration phase, R_d ,
 268 whereby $R_a = R_d = R/2$. The position of the slide, varies in time according to the
 269 relationship:

$$0 < t < T \begin{cases} x_s = x_0 + s(t) \cos(\varphi) \\ y_s = y_0 + s(t) \sin(\varphi) \end{cases} \quad (8)$$

270 where x_0, y_0 defines the start location and φ is the angle from the x-axis that the
 271 slide travels in, Acceleration phase:

$$s(t) = R_a \left[1 - \cos \left(\frac{u_{max}}{R_a} t \right) \right], \quad 0 < t < T_a \quad (9)$$

272 Deceleration phase:

$$s(t) = R_a + R_d \left[\sin \left(\frac{u_{max}}{R_d} (t - T_a - T_c) \right) \right], \quad T_a < t < T. \quad (10)$$

273 The width and height of the resulting half-sinusoid can be adjusted by altering
 274 the estimated run out distance of the slide and the estimated maximum velocity,
 275 respectively. Slide dimensions are specific to each scenario and are discussed in
 276 section 3 and 4. The slide height remains constant as it travels over the bathymetry,
 277 whereas in the case of a deformable slide, the slide material will move under gravity
 278 according to local slope and changes in thickness.

279 2.4. Generation of meshes and three-dimensional domains

280 A three-dimensional mesh was generated using QGIS software (QGIS Devel-
 281 opment Team, 2009), *qmesh* (Avdis et al., 2018) and *Gmsh* (Geuzaine and Remacle,

282 2009). The spatial resolution at the coastlines of interest is 0.5 km, and 1 km at other
283 coastlines, the resolution is linearly increased to 50 km furthest from the coastline.
284 In the initial location of the submarine slide the spatial resolution is 2 km within
285 a 80 km radius of the slide. Higher resolution is specified in shallow regions, and
286 coarser resolution in regions of deep ocean, by varying the resolution according to the
287 square-root of the bathymetry and gradient of the bathymetry. This is in order to
288 capture the reduction in wavelength when tsunami enter shallower water. Combining
289 these constraints on spatial mesh resolution results in mesh elements that have typ-
290 ical maximum edge lengths of 35 km. The mesh is composed of triangular elements
291 across a two-dimensional surface and is extruded down radially to the depth of the
292 bathymetry, with a single layer of elements, making this similar to a depth averaged
293 approach (Mitchell et al., 2010; Wells et al., 2010; Hill et al., 2014). A consequence
294 of this approximation is the requirement for a minimum water depth, here 10 m is
295 chosen. Multiple layers have been used in Fluidity, to capture dispersion in Oishi
296 et al. (2013) and in sensitivity tests in Smith et al. (2016) and Smith (2017). Future
297 work can incorporate multiple layers into the three-dimensional Single Material ap-
298 proach presented here. Bathymetric data was obtained from the GEBCO 250 (IOC,
299 2008) dataset. The coastline is represented by the 0 m contour extracted from the
300 GEBCO 250 dataset (IOC, 2008).

301 On the sea floor of the domain a no-normal flow boundary condition is applied
302 except where a velocity boundary condition is instead being used to mimic the effect
303 of the slide on the water during slide motion (Equation 6). A free surface boundary
304 condition (see Smith et al. (2016)) is applied to the upper surface of the domain,
305 but without movement of the mesh. The coastlines have a free-slip, no-normal flow
306 boundary condition, which prevent inundation and reflect incoming waves. The
307 minimum water depth in simulations is 10 m at the coastline, meaning that shoaling

308 at depths less than 10 m, and inundation are not captured in the model. As the waves
309 are not subject to the final shoaling that occurs, the wave amplitudes reported at
310 the coastlines will be less than expected wave amplitudes on land. At the open
311 boundaries surrounding the domain a ‘stress-free’ condition is used that allows the
312 waves to freely flow out of the domain. The water has a density of 1000 kgm^{-3} and
313 the kinematic viscosity tensor is isotropic and set to $1 \text{ m}^2\text{s}^{-1}$. These ‘eddy’ viscosity
314 values were selected in order to dampen any instabilities at the water surface, whilst
315 being low enough to have a negligible effect on the overall waveform.

316 **3. Model verification: test case in Gulf of Mexico**

317 *3.1. Set-up*

318 The two-dimensional submarine slide scenario in the Gulf of Mexico, that is
319 considered in Horrillo et al. (2013) and Smith et al. (2016), is here extended into
320 three dimensions following Horrillo et al. (2013), who used the TSUNAMI3D model.
321 TSUNAMI3D is a three-dimensional Navier–Stokes model for water and submarine
322 slide that builds on the classical VoF formulation of Hirt and Nichols (1981) to track
323 both the water surface and slide interface on a structured grid with a 3rd order fi-
324 nite difference scheme to solve the incompressible Navier–Stokes system. The VoF
325 method determines regions containing water and slide material, with corresponding
326 cell-weighted values of physical properties (density and viscosity) used in the mo-
327 mentum equation, in a very similar manner to the MM2FS approach employed in
328 this work. TSUNAMI3D uses a simplified treatment of the free surface: the free sur-
329 face in each column of cells is treated as horizontal, and consequently, wave breaking
330 cannot be modelled. The water and slide are modelled as two incompressible, Newto-
331 nian fluids. For the full-scale tsunami simulations in a vertical two-dimensional slice

332 domain TSUNAMI3D is configured to only employ two cells in the “third” dimen-
333 sion (Horrillo et al., 2013). This submarine slide is a hypothetical scenario based on
334 geomorphological evidence for an historic slide of that volume in the same area, with
335 parameters described in Table 2. The location and direction of failure (heading) of
336 the slide are shown in Figure 1A and the three-dimensional mesh is shown in Figure
337 1B.

338 To simulate a three-dimensional simplified rigid slide in this test case, the length
339 of the slide, L , and thickness, h , are kept consistent with the two-dimensional sim-
340 ulations in Smith et al. (2016) and Horrillo et al. (2013) and the maximum slide
341 height is then adjusted to give the same cross sectional area. The shape is shown in
342 Figure 1C. The two-dimensional slide thickness is maintained to a distance of $\pm B/2$
343 perpendicular to the transect line, in both directions, where B is the slide width,
344 18.1 km (Horrillo et al., 2013). A smoothing factor, $h_{\max} \exp - (0.3(\frac{y'}{B})^4)$, is applied
345 as a function of perpendicular distance, y' , to the transect line. This smoothing is
346 in line with Harbitz (1992) and Hill et al. (2014), except the factor of 0.3 which has
347 been altered from 2.0, to ensure a consistent slide volume with Horrillo et al. (2013)
348 of 26.7 km^3 (See Table 2 and Figure 1C). The horizontal axis of the two-dimensional
349 domain forms the transect through the centre of the slide, along the bearing of slide
350 failure.

351 The SM-DS-SV approach is modelled in three dimensions using the Boussinesq
352 set-up in Fluidity, as described in Section 2. For the SM-RS-EV approach, a slope
353 angle is required in Equation (7) to calculate the estimated velocity profile. The local
354 continental slope is averaged over the length of the slide and to a run-out distance of
355 one slide length (Table 2). The acceleration of the slide in the SM-RS-EV approach
356 is altered to match the acceleration of the slide in Horrillo et al. (2013) (Figure 2).
357 The timestep for all three approaches modelled in this test case is set at 1 s.

Table 2: Parameters for three-dimensional SM-RS-EV simulation in Gulf of Mexico. Where L is slide length and S is the smoothing length described in Section

4.1.						
Long, Lat of headwall	Heading	Slope Angle	Maximum veloc- ity (m/s)	Volume (km ³)	Slide thick- ness (m)	L,S,Width (km)
95:40:35W, 27:42:59N	168.15°	0.69°	41	26.7	96.65	16,9,4,18

358 3.2. Results

359 For each simulation using Fluidity (the SM-RS-EV, SM-RS-SV and SM-DS-SV
360 approaches) the generated waves are compared to TSUNAMI3D (Horrillo et al., 2013)
361 at 7 and 10 minutes after slide motion has initiated (Figure 3). At 7 minutes there is
362 a reduction in the maximum wave amplitude of about 50% in both TSUNAMI3D and
363 Fluidity’s SM-DS-SV approach in three dimensions compared to the maximum wave
364 amplitudes the models predict in two dimensions (Horrillo et al., 2013; Smith et al.,
365 2016), due to geometric/radial spreading, showing the importance of performing
366 three-dimensional modelling.

367 In three dimensions, there is a good match between the three Fluidity approaches
368 and TSUNAMI3D (Figure 3). TSUNAMI3D predicts a maximum peak-to-trough
369 amplitude of 44 m. At this time, the SM-RS-EV and SM-RS-SV approaches produce
370 almost identical wave forms to each other, predicting a peak-to-trough amplitude of
371 49 m. The SM-DS-SV approach predicts a smaller peak-to-trough amplitude of 37
372 m. Although the positive wave height produced by the SM-DS-SV approach is larger
373 than for the SM-RS approach, the waves generated in the SM-RS approach have
374 a deeper trough, resulting in a larger peak-to-trough amplitude. TSUNAMI3D’s
375 peak-to-trough amplitude falls within the range of Fluidity peak-to-trough am-
376 plitudes (35–49 m). At 7 minutes, the best match to TSUNAMI3D in terms of
377 maximum and minimum wave amplitude is the SM-DS-SV approach. This is ex-

378 pected as the slide modelled in TSUNAMI3D also deforms, allowing the slide length
379 to increase. The SM-DS-SV approach generates greater wave amplitudes than the
380 SM-RS-EV and SM-RS-SV approaches because the deformation of the slide causes
381 an increase in slide thickness at the front of the slide.

382 At 10 minutes there is still a qualitatively good match between TSUNAMI3D
383 and all Fluidity approaches. Although Horrillo et al. (2013) do not give quantitative
384 details of wave heights, the maximum wave amplitude in TSUNAMI3D appears to
385 be under 20 m (and the minimum wave amplitude greater than -30 m). All Fluidity
386 approaches produce a maximum wave height of 12.5–13 m. In TSUNAMI3D the
387 maximum wave height occurred at 7 minutes and by 10 minutes, the wave height
388 had decreased. In Fluidity maximum wave heights are observed during the slide
389 acceleration phase at 8 min 28 s, 8 min 32 s, and 7 min 40 s for SM-RS-EV, SM-RS-SV
390 and SM-DS-SV approaches respectively, which is in agreement with TSUNAMI3D.
391 Over the course of the simulation, the SM-RS-EV approach predicts a maximum
392 wave height that is 16 % lower than the maximum wave height that the SM-DS-SV
393 approach predicts. Compared to TSUNAMI3D all approaches slightly underestimate
394 the maximum positive wave amplitude, future work could investigate whether this
395 could be due to the exclusion of the tangential applied stress (skin friction drag) in
396 these SM approaches in three dimensions.

397 **4. Atlantic Ocean Scenarios**

398 Considering the potential for another tsunamigenic slide in the Norwegian-Greenland
399 Sea, two hypothetical submarine slide events at the continental margin, west of Scot-
400 land and Ireland, on the edge of the Atlantic Ocean, were simulated in three dimen-
401 sions. These locations were identified as having the potential to fail in the future,
402 based on sedimentological evidence of historic slides and evidence of high sedimen-

403 tation rates. Several other locations in the Norwegian-Greenland Sea have also been
404 identified as having the potential to fail, but the two scenarios investigated here were
405 chosen due to their proximity to land. The two slides occur on either side of the
406 Rockall Trough basin (seen in Figure 4). The Peach Slide Complex is found on the
407 eastern slope of the trough, on the Barra Fan, and the Rockall Bank slide scenario
408 occurs on the opposite slope on the trough, on the western side.

409 Submarine slide geometry and motion for the hypothetical scenarios in the Norwegian-
410 Greenland Sea were estimated using typical dimensions for submarine slides in the
411 Atlantic Ocean (Hühnerbach and Masson, 2004). Scenario 1, named Rockall Bank,
412 is based on the occurrence of a past failure on the eastern flank (Roberts, 1972;
413 Georgiopoulou et al., 2013; Salmanidou et al., 2017). Scenario 2, named Peach Slide,
414 is located on the Barra-Donegal Fan where the complex shows evidence of about
415 four separate submarine slide events with slide volumes ranging from 135–673 km³
416 (Holmes et al., 1998). The two slides have motions in approximately opposite direc-
417 tions. This will allow the effect of slide direction on the waves generated to be estab-
418 lished. Volumes of historical submarine slides in this area are not well constrained.
419 Salmanidou et al. (2015) considered slides on the Rockall bank with volumes ranging
420 from 265-765 km³. For both scenarios, failure volumes of 100 km³ are used and are
421 considered conservative estimates, not “worse case” scenarios.

422 *4.1. Set-up*

423 The dimensions of the hypothetical slides considered in this section must be
424 estimated. The rationale for estimating slide dimensions is based on the previous
425 work of Harbitz (1992), Løvholt et al. (2005) and Hill et al. (2014). In the model,

426 the slide thickness h_s is defined as:

$$h_s = \begin{cases} h_{\max} \left(\exp - \left(2 \left(\frac{x'+S+L}{S} \right)^4 \right) - \left(2 \frac{y'}{B} \right)^4 \right) & \text{for } -(L+2S) < x' < -(L+S) \\ h_{\max} \left(\exp - \left(2 \frac{y'}{B} \right)^4 \right) & \text{for } -(L+S) \leq x' < -S \\ h_{\max} \left(\exp - \left(2 \left(\frac{x'+S}{S} \right)^4 \right) - \left(2 \frac{y'}{B} \right)^4 \right) & \text{for } -S \leq x' < 0 \end{cases} \quad (11)$$

where the slide has dimensions of maximum height, h_{\max} , length, L , and width, B . A smoothing length, S , is used along the edges of the slide to avoid sharp edges, which give rise to numerical oscillations, as described in Harbitz (1992). x' and y' are the transverse and longitudinal coordinates, respectively, on a local plane aligned in the direction of slide motion φ :

$$x' = (x - x_s) \cos \varphi + (y - y_s) \sin \varphi \quad (12a)$$

and

$$y' = (x - x_s) \sin \varphi + (y - y_s) \cos \varphi \quad (13a)$$

427 where x_s and y_s are the coordinated of the back of the slide, and x and y are the
428 model coordinates in the Universal Transverse Mercator projection (UTM zone 30N).

Using these slide dimensions, h_{\max} , L and B , gives a total volume of the slide, V :

$$V = 0.9 B h_{\max} (L + 0.9 S), \quad (\text{Harbitz, 1992}). \quad (14a)$$

429 Values for V , L , S , B and h_{\max} are determined by fitting a power law to data
430 for the Atlantic Ocean collated in Hühnerbach and Masson (2004) and choosing
431 dimensions that fit the line based on four principles:

- 432 1. a desired slide volume, V
- 433 2. S , the smoothing/tapering length is defined as $L/2$

434 3. a relationship between V and B determined from Hühnerbach and Masson
435 (2004):

$$V = 0.0335 \times B^{2.373} \quad (R^2 = 0.9) \quad (15)$$

436 4. a relationship between L and B determined from Hühnerbach and Masson
437 (2004):

$$(L + 2S) = 1.377 \times B^{-1.11} \quad (R^2 = 0.9) \quad (16)$$

438 where R^2 is a measure of how well the line of best fit fits the observational data. The
439 resulting three-dimensional slide is shown in Figure 4B.

440 The MM2FS approach (Smith et al., 2016) is used to model the Rockall Bank and
441 Peach slides in two dimensions, modelling the slide and water as viscous fluids. Both
442 two-dimensional slide geometries are determined from a three-dimensional volume of
443 100 km^3 . Fitting a power law to the data for slides the Atlantic Ocean in Hühnerbach
444 and Masson (2004) and choosing slide dimensions to fit the line, results in a slide
445 length of 58 km, a maximum slide thickness of 91 m (this agrees with estimated
446 headscarp heights from Georgiopoulou et al. (2013) of 50–150 m) and a slide width
447 of 29.1 km (set out in Table 3). Two-dimensional multi-scale meshes are used (Figure
448 5). The slide shape through time is extracted from MM2FS simulations (Smith et al.,
449 2016) for use in the SM-DS-SV approach (Figures 6 and 7). The displacement of the
450 slide’s centre of mass is extracted for the SM-RS-SV approach. For the Rockall Bank
451 scenario, the SM-DS-SV approach (R1) and SM-RS-SV (R2) approach are applied,
452 along with two different estimated velocity profiles for the SM-RS-EV approach (R3
453 and R4). One velocity profile has a maximum velocity of 74 ms^{-1} (for constant slope
454 2.2° , R4) and the other has a maximum velocity of 29 ms^{-1} (constant slope 0.7° ,
455 R3), and consequently a much lower initial acceleration (Figure 8). The maximum

Table 3: Parameters for three dimensional simulations, Atlantic Ocean scenarios. The average slope was used to calculate the maximum velocity of the slide.

Scenario Name	Rockall Bank				Peach
Simulation Name	R1	R2	R3	R4	P1
Fluidity Approach	SM-DS-SV	SM-RS-SV	SM-RS-EV	SM-RS-EV	SM-DS-SV
Volume (km ³)	100				
Slide thickness (m)	91				
L,S, Width (km)	29, 14.5, 29.1				
Run-out length (km)	58				
Headwall Lon, Lat	13:15:13.86W, 57:10:16.95N				9:08:26.50W, 56:45:10.79N
Heading (°)	170				340
Average Slope (m/m)	0.7		2.2		0.67
Max Velocity (m/s)	Simulated	29	74	Simulated	

456 velocities for these velocity profiles were obtained through extracting bathymetry
457 data, the range of slopes found on the Rockall Bank (0.7–2.2 depending on the loca-
458 tion and length of the slope) and the force-balance question in section 2. Comparing
459 waves generated by slides with different accelerations and maximum velocities allows
460 the importance of slide deformation and velocity/acceleration to be considered. For
461 context, the slide in the Gulf of Mexico example has a maximum velocity of approx-
462 imately 45 ms⁻¹ (Figure 2). For the Peach slide the SM-DS-SV approach (P1) is
463 applied for comparison with the Rockall Bank using the same approach (SM-DS-SV)
464 to investigate the effect of direction on coastal hazard (R1).

465 The meshes for the Rockall Bank and Peach Slide have 151892 and 150257 nodes,
466 respectively (Figure 9). The timestep for the SM-RS-EV approach is 3 s (R3, R4),
467 and for the SM-RS-SV approach (R2) and for the SM-DS-SV approach the timestep
468 is 1 s (R1). For the SM-RS-EV approach (R3, R4) there is a negligible difference
469 in the resultant waves using a timestep of 1 s and 3 s. However for the SM-DS-SV
470 (R1, P1) and SM-RS-SV (R2) approaches, a smaller timestep of 1 s is required to
471 ensure stability due to sharper changes in vertical velocity across shorter length scales
472 compared to the smoothed rigid slide. Several numerical wave gauges are placed in
473 the domain to measure the variation of fields (including free surface height and
474 velocities) at specific geographic locations; e.g., between the slide and the coastlines
475 of Ireland, Northern Ireland and Scotland (Figure 4), and located radially around
476 the slide locations and the UK coast.

477 *4.2. Results and Discussion*

478 Simulations were run in parallel, on 48-256 cores, for a total simulation time
479 of 240 hours. The SM-RS-EV approach (R3, R4) took approximately 4000–4500
480 CPU hours (no. cores \times time to complete), the SM-RS-SV approach (R2) took
481 about 1.5 times as long, at 6500 CPU hours and the SM-DS-SV (R1, P1) approach
482 took approximately 4 times as long as the SM-RS-EV approach (R3, R4) at 18000
483 CPU hours. This is mostly due to the smaller timestep needed in the SM-DS-SV
484 approach (R1, P1) and the more complex velocity patterns present in the SM-RS-
485 SV (R2) and SM-DS-SV (R1, P1) approaches compared to the SM-RS-EV approach
486 (R3, R4). The SM-DS-SV approach (R1, P1) also required additional input files
487 and interpolations of the slide shape in space and time, adding additional overhead.
488 Throughout the simulations maximum wave amplitudes reach between 16 and 26
489 m in the wave generation region. However, for the majority of the domain wave

490 amplitudes are less than 10 m. Initially the results produced for the Rockall Bank
491 scenario using the SM-DS-SV, SM-RS-SV, and SM-RS-EV approaches are considered
492 (R1-R4). In this section the effect of slide velocity, acceleration and deformation on
493 the generated wave are considered.

494 *4.2.1. Rockall Bank: Comparison of model approaches, R1, R2, R3, R4*

495 The wave pattern generated over time by the SM-RS-SV and SM-DS-SV ap-
496 proaches for the Rockall Bank is presented (Figure 10). Waves propagate from the
497 generation zone and their amplitudes decay with increasing distance because of geo-
498 metric spreading and dispersion. As the waves propagate they are diffracted around
499 various seamounts, and later on, refracted around the Outer Hebrides. These wave
500 processes create constructive and deconstructive wave interference. Waves hit the
501 continental slope at ~ 30 mins and undergo shoaling (Figure 10). Shoaling leads to a
502 decrease in wavelength and wave speed, and an increase in wave amplitudes. Follow-
503 ing shoaling, both waves decay in amplitude whilst travelling over the continental
504 shelf and consequently waves between 1–10 m in amplitude reach just offshore of the
505 coastline (Figure 11). Waves reach land around 1 hour after the initiation of slide
506 motion and the first wave to reach land is a peak, and is followed by a trough. Waves
507 greater than 1 m in amplitude reach the coast of the mainland north western Irish
508 coast (Figure 11). The Outer Hebrides experiences wave heights of greater than 10–
509 20 m (depending on the use of the SM-RS-SV approach or the SM-DS-SV approach,
510 taking the brunt of the waves and sheltering much of mainland Scotland from expe-
511 riencing wave heights greater than a few metres. The north coast of Scotland records
512 waves 0.5–5 m in amplitude. Further afield, waves greater than 1 m in amplitude
513 reach the coast of Iceland and the Faroe Islands for both scenarios (Figure 11).

514 *4.2.2. Effect of slide deformation: SM-DS-SV (R1) vs. SM-RS-SV (R2)*

515 The SM-RS-SV (R2) and SM-DS-SV (R1) approaches exhibit very similar wave
516 patterns within the first 10 minutes after slide initiation (Figure 10). This suggests
517 that the wave pattern is primarily controlled by the slide motion, since the SM-RS-
518 SV (R2) approach assumes the slide is moving at the same speed as the slide's centre
519 of mass in the SM-DS-SV (R1) approach. The differences between the results can
520 be attributed to the internal slide deformation that occurs in the SM-DS-SV (R1)
521 approach and not in the SM-RS-SV (R2) approach. After the first 10 minutes, a
522 more complex wave pattern (more peaks and troughs) is produced by the SM-DS-
523 SV approach. The SM-DS-SV (R1) approach accounts for internal slide deformation
524 that generates additional short wavelength perturbations within the long wavelength
525 signal. This leads to velocity variations over the length of the slide in the SM-DS-SV
526 approach contributing to wave generation in additional locations. In the SM-RS-
527 SV (R2) approach the slide surface is smooth, there is no internal deformation, and
528 therefore vertical velocity is only induced at the front and back of the slide (elsewhere
529 the thickness is constant). The SM-RS-SV (R2) approach generates waves with lower
530 amplitudes than the SM-DS-SV (R1) approach (Figure 11), which suggests the de-
531 formation of the slide is contributing to increased wave heights. Another explanation
532 for the difference in wave heights generated by the two different approaches is that
533 the velocity of the slide in the SM-RS-SV (R2) approach (which uses the velocity of
534 the centre of mass on the slide) is not a good approximation for the side motion in
535 the SM-DS-SV (R1) approach, in which different sections of the slide will move at
536 different velocities.

537 In this example, slide deformation leads to an increase in wave heights at the
538 coastline. This increase in wave amplitude depends on the location of the wave

539 gauge, but in general, the SM-DS-SV approach produces $\sim 30\text{--}50\%$ higher waves
540 than the SM-RS-SV approach and two times greater maximum wave amplitudes.
541 These findings are in agreement with Grilli and Watts (2005) who report increases
542 in wave amplitudes at wave gauges of between 13–35% and an increase in wave run
543 up of a factor of 2–3 for deformable slides compared to rigid slides. Grilli and Watts
544 (2005) conclude that intense slide deformation at shallow water depths significantly
545 increases the coastal hazard the waves pose. However, other studies have found that
546 slide deformation does not have a significant effect on the generated wave ampli-
547 tude compared to rigid slides (Løvholt et al., 2015), because the slide accelerates
548 too fast into deeper water for the deformation to influence the wave generation. In
549 the scenarios considered here, slide deformation does contribute to wave generation.
550 Some studies have found that slide deformation leads to decreased wave amplitudes
551 (Watts, 1997; Ataie-Ashtiani and Najafi-Jilani, 2008; Kirby et al., 2016). However,
552 the majority of these studies consider submarine slides at laboratory scale, higher
553 slope angles ($15\text{--}60^\circ$) and slides that are smaller, have a higher thickness to length
554 ratio and different slide rheologies (e.g granular and confined granular) (Watts, 1997;
555 Ataie-Ashtiani and Najafi-Jilani, 2008). Although the example in Kirby et al. (2016)
556 is full scale and three dimensional, the scenario considered two separate, but simul-
557 taneous slides, whose combined effects generate the wave, and therefore it is difficult
558 to compare the results with the single slide scenarios considered here.

559 *4.2.3. Effect of slide velocity and acceleration: SM-RS-EV using different velocity*
560 *profiles (R3 vs. R4)*

561 The resultant waves from two rigid slides moving with two different velocities
562 profiles are also considered (Fig. 11). The wave heights predicted by the SM-RS-EV
563 simulation, representing a slow slide moving with a maximum velocity of 29 ms^{-1}

564 (R3) are, in places, a fraction of (or even negligible compared to) the wave amplitudes
565 generated by the rigid fast slide moving with a maximum velocity of 74 ms^{-1} (R4,
566 fast). The increase in maximum velocity is approximately a factor of 2.5, but the
567 waves generated can be a factor of 3–7 times bigger. This suggests that the wave is
568 very sensitive to the slide and acceleration of the slide generating the waves. At the
569 coast, the maximum wave recorded at each location is 2–20 times larger for the faster
570 slide (R4), depending on precise location. This strong dependence of wave amplitude
571 on slide velocity and acceleration is in agreement with many previous findings, e.g.
572 Wiegel (1955); Watts (1998, 2000); Watts et al. (2000); Ward (2001); Tinti et al.
573 (2001); Haugen et al. (2005); Løvholt et al. (2005); Harbitz et al. (2006).

574 *4.2.4. Application to coastal hazard assessments*

575 Waves with amplitudes of up to 10 m from the Rockall Bank and Peach slides
576 reach the coastline after undergoing shoaling on the continental slope. The highest
577 waves that reach the coast are recorded along the west coast of Ireland for both
578 slides, with peak heights of 10 m for the Peach slide and around 4 m for the Rockall
579 slide. Just offshore the Northern Irish city of Londonderry/Derry waves are predicted
580 between 2–4.5 m high for Peach Slide and 1.2–2 m high from Rockall Bank slide
581 (Figure 12). The city is sheltered by the surrounding coastline and therefore is not
582 affected by waves of high amplitude. However, in Lough Foyle, further shoaling at
583 shallow water depths may result in increased wave amplitudes. Wave heights are
584 generally low ($<1 \text{ m}$) along the south-western Scottish mainland coast, but start to
585 peak again around the islands of Arran, and Islay (point e on Fig. 4). The Outer
586 Hebrides experience similar height waves from both the Peach and Rockall slides,
587 but with slightly higher peaks for the Peach scenario (just over 4m vs. just over 3
588 m respectively). Along the northern coast of Scotland (f to g on Fig. 4) the Rockall

589 scenario produces large maximum wave heights, but these are generally low (peak
590 2.25 m) with the Peach slide producing a maximum wave height of 2 m.

591 The Peach slide produces larger peak amplitude waves in the direction of slide
592 travel at 100 km distance from the slide starting point, but these seem to rapidly
593 diminish in size (Fig. 12). At 200 km from the slide start point both slide scenarios
594 produce similar sized peak waves, that are again aligned with the slide direction.
595 The Rockall slide appears to have a very clear focus of energy with clear dips in
596 wave amplitude perpendicular to slide direction. In contrast, the energy from the
597 Peach slide spreads more evenly in all directions (but with a peak aligned to the slide
598 direction).

599 *4.2.5. Limitations*

600 There are limitations to the results presented here. Firstly, the MM2FS simu-
601 lations show that some slide deformation occurs at scales on the order of 100 m.
602 However, the three-dimensional simulations have a minimum mesh resolution in the
603 slide region of 2 km, meaning that the slide is described by approximately 423 el-
604 ements (for all approaches). Therefore the three-dimensional SM-DS-SV (R1, P1)
605 simulations may be missing, or smoothing out, more detailed information about the
606 slide geometry. Mesh resolution studies are recommended to investigate to what ex-
607 tent this affects the waves generated. Resolution studies have previously only been
608 completed for the SM-RS-EV approach simulations by Hill et al. (2014), where it
609 was concluded that multi-scale meshes with the same minimum and maximum edge
610 lengths as those considered here were able to accurately represent observed run-up
611 height estimates.

612 Secondly, the slides here are also assumed to be constant width and, in reality,
613 there will be some spreading or funnelling of the slide laterally. The velocity boundary

614 condition, that mimics the slide deformation and motion, is also applied uniformly
615 along the width, whereas in reality there will be differences in bathymetry across the
616 width of the slide which will lead to changes in deformation along the width of the
617 slide. If deformation is permitted in three dimensions, this may also have an effect
618 on the difference between waves amplitudes generated by rigid and deformable slides.
619 In previous experimental work (Watts et al., 2005), the slide width has been found to
620 have an important effect on wave amplitude, therefore a more thorough investigation
621 including modelling of slides that are able to spread laterally, should be performed
622 in order to establish to what degree this has an effect on the generated wave. If, in
623 the results presented here, thickening of the front of the slide is increased compared
624 to if the slide was allowed to spread laterally, this could account for some of the
625 increased wave heights seen by the SM-DS-SV approach compared to the SM-RS-SV
626 approach.

627 Lastly, the configuration employed here does not allow inclusion of shoaling and
628 inundation in areas of bathymetry shallower than 10 m depth near to the coastlines.
629 This means that wave heights recorded at the wave gauges are likely underestimated
630 as the final shoaling and funnelling is not modelled. Inundation modelling within
631 Fluidity is too computationally expensive to fall within the scope of this study.
632 An alternative approach is to use another model, such as TELEMAC or Thetis
633 (Kärnä et al., 2018; Pan et al., 2019, 2020), to simulate inundation by forcing it with
634 the output of Fluidity. This is recommended as future work to fully establish the
635 magnitude of the underestimation of wave amplitudes.

636 5. Conclusions

637 A three-dimensional Navier-Stokes model (using the Boussinesq approximation)
638 has been presented that simulates the tsunami waves generated by submarine slides.

639 The framework has been used to investigate the role of slide deformation in wave
640 generation. In the model, the water motion was driven by a boundary condition
641 applied at the sea floor. The boundary condition mimicked the effect of the slide
642 motion on the water column, and was determined in three different ways, using 1)
643 a submarine slide modelled as a viscous fluid, without fixed shape, moving under
644 gravity, 2) a rigid submarine slide, moving with a velocity profile extracted from (1)
645 and 3) a rigid submarine slide, moving with a prescribed analytical velocity profile.
646 For methods 1) and 2) a two-dimensional simulation was used to model both the
647 submarine slide and water as viscous fluids. The simulations were then ‘coupled’;
648 i.e., outputs (change in shape and motion of submarine side material) from a 2D
649 simulation of viscous fluids was extracted and used as a boundary condition for the
650 three-dimensional simulation of water.

651 We verified our model, framework and coupling methodology by comparing our
652 results to a previous simulation of a tsunamigenic submarine slide in the Gulf of
653 Mexico. We then showed the difference in risk due to the consideration of slide
654 deformation for hypothetical submarine slides around the UK (with the limitation of
655 modelling wave propagation to 10 m depth off shore). Shoaling at depths less than
656 10 m, and inundation are not captured in the model. As the waves are not subject
657 to the final shoaling that occurs, the wave amplitudes reported at the coastlines will
658 be less than the expected wave amplitudes on land.

659 Comparisons were made between an approach that accounts for deformation of
660 submarine slides (1) and an approach that used a rigid slide that moved according
661 to prescribed motion (3). Slides moving with greater velocity and acceleration pro-
662 duce larger amplitude waves and results show there is a strong dependence of wave
663 amplitude on velocity and acceleration. Approaches that do not consider slide defor-
664 mation appear to provide good estimates compared to approaches that do account

665 for slide deformation. However, it is still imperative to use accurate estimates for
666 the slide velocity and position throughout the wave generation process, because the
667 wave characteristics are very sensitive to these parameters. Since it is difficult to
668 measure submarine slide velocities as they occur, numerical modelling of slides is a
669 useful tool to obtain good estimates for these parameters, which could then be used
670 as an input for a ocean-scale model.

671 In this work, slide deformation was modelled assuming that the slide behaved as
672 a viscous fluid. The deformation of slide material caused slide thickness to increase
673 and decrease along the length of the slide. The slide thickness increased up to 4
674 times larger than its starting thickness, and there is a corresponding decrease in
675 thickness at other areas of the slide in accordance with volume conservation. The
676 slope varies along the length of the slide which causes material to move at different
677 velocities, resulting in local thickening and thinning. Results presented here found
678 that changes in slide thickness contribute to a 30-50% increase in wave height for
679 a slide that deforms compared to a rigid slide. However, modelling the slide as a
680 viscous fluid may not result in the most accurate representation of slide dynamics
681 and future work should investigate more. Furthermore, lateral spreading of the slide
682 is not considered in this study and this could alter the effect of slide deformation,
683 as the slide material spreads sideways. Multi-material simulations presented here
684 indicate that components of slide deformation that occur at shallower depths, on the
685 steepest slopes and involving the largest volume are more energetic than deformation
686 at other sections of the slide and contributes most to wave generation. This work
687 offers a new methodology for simulating oceanic-scale tsunamis caused by submarine
688 slides within the same numerical framework, without recourse to coupling several
689 different models together. In this study two-dimensional simulations were required to
690 test the model, but in future simulations, the slide dynamics can be estimated given

691 information about the slope angle and slide geometry. It provides the possibility for
692 exploring the risk posed by tsunamigenic submarine slides, which threaten coastlines
693 not normally thought to be prone to tsunamis.

694 Future work should model slides that spread laterally, and investigate the effect
695 this has on wave amplitudes and on the relative significance of slide deformation. The
696 effect of lateral spreading on the conclusions drawn here is unknown but potentially
697 significant.

698 **6. Acknowledgements**

699 JH, GC and MDP acknowledge funding from NERC under project (NE/K000047/1).
700 The authors would like to acknowledge the use of the Imperial College London HPC
701 service. We would like to thank two anonymous reviewers for very helpful reviews
702 that improved this manuscript.

703 **7. References**

704 **References**

- 705 Abadie, S., Morichon, D., Grilli, S., Glockner, S., 2010. Numerical Simulation of Waves Generated by Landslides using a Multiple-
706 Fluid Navier–Stokes Model. *Coastal Engineering* 57, 779–794. URL: <http://linkinghub.elsevier.com/retrieve/pii/S0378383910000396>,
707 doi:10.1016/j.coastaleng.2010.03.003.
- 708 Abadie, S.M., Harris, J.C., Grilli, S.T., Fabre, R., 2012. Numerical Modeling of Tsunami Waves Generated by the Flank Collapse of
709 the Cumbre Vieja Volcano (La Palma, Canary Islands): Tsunami Source and Near Field Effects. *Journal of Geophysical Research*
710 117, C05030. URL: <http://www.agu.org/pubs/crossref/2012/2011JC007646.shtml>, doi:10.1029/2011JC007646.
- 711 AMCG, 2014. Fluidity manual v4.1.11, Imperial College London.
- 712 Assier-Radkiewicz, S., Einrich, P.H., Abatier, P.C.S., Avoye, B.S., 2000. Numerical Modelling of a Landslide-Generated Tsunami :
713 The 1979 Nice Event. *Pure and Applied Geophysics* 157, 1707–1727.
- 714 Assier-Rzadkiewicz, S., Mariotti, C., Heinrich, P., 1997. Numerical Simulation of Submarine Landslides and
715 their Hydraulic Effects. *Journal of Waterway, Port, Coastal, and Ocean Engineering* 123, 149–157. URL:
716 [http://ascelibrary.org/doi/abs/10.1061/\(ASCE\)0733-950X\(1997\)123:4\(149\)](http://ascelibrary.org/doi/abs/10.1061/(ASCE)0733-950X(1997)123:4(149)).
- 717 Ataie-Ashtiani, B., Najafi-Jilani, A., 2008. Laboratory Investigations on Impulsive Waves caused by Underwater Landslide. *Coastal En-*
718 *gineering* 55, 989–1004. URL: <http://linkinghub.elsevier.com/retrieves/pii/S0378383908000586>, doi:10.1016/j.coastaleng.2008.03.003.

- 719 Ataie-Ashtiani, B., Shobeyri, G., 2008. Numerical Simulation of Landslide Impulsive Waves by Incompressible Smoothed Particle Hydrodynamics. *International Journal for Numerical Methods in Fluids* , 209–232 URL: <http://onlinelibrary.wiley.com/doi/10.1002/flid.1526/abstract>, doi:10.1002/flid.
- 720
721
- 722 Avdis, A., Candy, A., Hill, J., Kramer, S., Piggott, M., 2018. Efficient unstructured mesh generation for marine renewable energy applications. *RENEWABLE ENERGY* 116, 842–856. URL: <http://dx.doi.org/10.1016/j.renene.2017.09.058>, doi:10.1016/j.renene.2017.09.058.
- 723
724
- 725 Bondevik, S., Løvholt, F., Harbitz, C., Mangerud, J., Dawson, A., Inge Svendsen, J., 2005a. The Storegga Slide Tsunami—Comparing Field Observations with Numerical Simulations. *Marine and Petroleum Geology* 22, 195–208. URL: <http://linkinghub.elsevier.com/retrieve/pii/S0264817204001904>, doi:10.1016/j.marpetgeo.2004.10.003.
- 726
727
- 728 Bondevik, S., Mangerud, J., Dawson, S., Dawson, A., Lohne, Ø., 2005b. Evidence for Three North Sea Tsunamis at the Shetland Islands Between 8000 and 1500 Years Ago. *Quaternary Science Reviews* 24, 1757–1775. URL: <http://www.sciencedirect.com/science/article/pii/S0277379105000739>, doi:10.1016/j.quascirev.2004.10.018.
- 729
730
- 731 Bornhold, B., Thomson, R., 2012. Tsunami Hazard Assessment Related to Slope Failures in Coastal Waters. *Landslides—Types, Mechanisms and Modeling*, edited by: Clague, JJ and Stead, D., Cambridge University Press , 108–120.
- 732
- 733 Bryn, P., Solheim, A., Berg, K., Lien, R., Forsberg, C., Hafidason, H., Ottesen, D., Rise, L., 2003. The Storegga Slide Complex; Repeated Large Scale Sliding in Response to Climatic Cyclicality, in: Locat, J., Mienert, J., Boisvert, L. (Eds.), *Submarine Mass Movements and Their Consequences*. Springer Netherlands. volume 19 of *Advances in Natural and Technological Hazards Research*, pp. 215–222.
- 734
735
736
- 737 Bugge, T., Belderson, R., Kenyon, N., 1988. The Storegga Slide. *Philosophical Transactions of the Royal Society London* 325, 357–388. URL: <http://www.jstor.org/stable/10.2307/38068>.
- 738
- 739 Capone, T., Panizzo, A., Monaghan, J.J., 2010. SPH Modelling of Water Waves Generated by Submarine Landslides. *Journal of Hydraulic Research* 48, 80–84. URL: <http://www.tandfonline.com/doi/abs/10.1080/00221686.2010.9641248>, doi:10.1080/00221686.2010.9641248.
- 740
741
- 742 Dawson, A., Long, D., Smith, D., 1988. The Storegga Slides: Evidence from eastern Scotland for a Possible Tsunami. *Marine Geology* 82, 271–276. URL: <http://www.sciencedirect.com/science/article/pii/0025322788901466>, doi:10.1016/0025-3227(88)90146-6.
- 743
- 744 De Blasio, F., Elverhøi, A., Issler, D., Harbitz, C., Bryn, P., Lien, R., 2005. On the Dynamics of Subaqueous Clay Rich Gravity Mass Flows—The Giant Storegga Slide, Norway. *Marine and Petroleum Geology* 22, 179–186. URL: <http://linkinghub.elsevier.com/retrieve/pii/S0264817204001886>, doi:10.1016/j.marpetgeo.2004.10.014.
- 745
746
- 747 Fine, I., Rabinovich, A., Bornhold, B., Thomson, R., Kulikov, E., 2005. The Grand Banks Landslide-Generated Tsunami of November 18, 1929: Preliminary Analysis and Numerical Modeling. *Marine Geology* 215, 45–57. URL: <http://linkinghub.elsevier.com/retrieve/pii/S002532270400324X>, doi:10.1016/j.margeo.2004.11.007.
- 748
749
- 750 Fine, I., Rabinovich, A., Kulikov, E., Thomson, R., Bornhold, B., 1998. Numerical Modelling of Landslide-generated Tsunamis with Application to the Skagway Harbor Tsunami of November 3, 1994, in: *Proc. Int. Conf. on Tsunamis*, Paris, pp. 211–223.
- 751
- 752 Gauer, P., Elverhøi, A., Blasio, F.D., 2006. On Numerical Simulations of Subaqueous Slides: Back-calculations of Laboratory Experiments. *Norwegian Journal of Geology* 86, 295–300.
- 753
- 754 Gauer, P., Kvalstad, T.J., Forsberg, C.F., Bryn, P., Berg, K., 2005. The Last Phase of the Storegga Slide: Simulation of Retrogressive Slide Dynamics and Comparison with Slide-Scar Morphology. *Marine and Petroleum Geology* 22, 171–178. URL: <http://linkinghub.elsevier.com/retrieve/pii/S0264817204001874>, doi:10.1016/j.marpetgeo.2004.10.004.
- 755
756

- 757 Georgiopoulou, A., Shannon, P.M., Sacchetti, F., Haughton, P.D.W., Benetti, S., 2013. Basement-controlled
758 multiple slope collapses, Rockall Bank Slide Complex, NE Atlantic. *Marine Geology* 336, 198–214. URL:
759 <http://www.sciencedirect.com/science/article/pii/S002532271200312X>, doi:10.1016/j.margeo.2012.12.003.
- 760 Geuzaine, C., Remacle, J.F., 2009. Gmsh: A 3-D finite element mesh generator with built-in pre- and post-processing facilities.
761 *International journal for numerical methods in engineering* 79, 1309–1331. doi:10.1002/nme.2579.
- 762 Glimsdal, S., Pedersen, G.K., Harbitz, C.B., Løvholt, F., 2013. Dispersion of Tsunamis: Does it Really Matter? *Nat. Hazards Earth*
763 *Syst. Sci.* 13, 1507–1526. URL: <http://www.nat-hazards-earth-syst-sci.net/13/1507/2013/>, doi:10.5194/nhess-13-1507-2013.
- 764 Grilli, S., Watts, P., 2005. Tsunami Generation by Submarine Mass Failure. I: Modeling, Experimental Validation, and Sensitivity
765 Analyses. *Journal of Waterway, Port, Coastal, and Ocean Engineering* 131, 283–297.
- 766 Harbitz, C.B., 1992. Model Simulations of Tsunamis Generated by the Storegga Slides. *Marine Geology* 105, 1–21. URL:
767 <http://www.sciencedirect.com/science/article/pii/002532279290178X>.
- 768 Harbitz, C.B., Løvholt, F., Pedersen, G., Masson, D.G., 2006. Mechanisms of Tsunami Generation by Submarine Landslides: A Short
769 Review. *Norsk Geologisk Tidsskrift* 86, 255.
- 770 Harbitz, C.B., Løvholt, F., Bungum, H., 2014. Submarine landslide tsunamis: how extreme and how likely? *Natural Hazards* 72,
771 1341–1374. URL: <http://link.springer.com/10.1007/s11069-013-0681-3>, doi:10.1007/s11069-013-0681-3.
- 772 Haugen, K.B., Løvholt, F., Harbitz, C.B., 2005. Fundamental Mechanisms for Tsunami Generation by Submarine Mass Flows in Ide-
773 alised Geometries. *Marine and Petroleum Geology* 22, 209–217. URL: <http://linkinghub.elsevier.com/retrieve/pii/S0264817204001916>,
774 doi:10.1016/j.marpetgeo.2004.10.016.
- 775 Hiester, H.R., Piggott, M.D., Allison, P.A., 2011. The Impact of Mesh Adaptivity on the Gravity Current Front Speed in a Two-
776 Dimensional Lock-Exchange. *Ocean Modelling* 38, 1–21. URL: <http://www.sciencedirect.com/science/article/pii/S1463500311000060>,
777 doi:10.1016/j.ocemod.2011.01.003.
- 778 Hill, J., Collins, G.S., Avdis, A., Kramer, S.C., Piggott, M.D., 2014. How Does Multiscale Modelling and Inclusion of Real-
779 istic Palaeobathymetry Affect Numerical Simulation of the Storegga Slide Tsunami? *Ocean Modelling* 83, 11–25. URL:
780 <http://www.sciencedirect.com/science/article/pii/S1463500314001164>, doi:10.1016/j.ocemod.2014.08.007.
- 781 Hill, J., Piggott, M.D., Ham, D.A., Popova, E.E., Srokosz, M.A., 2012. On the Performance of a Generic Length
782 Scale Turbulence Model Within an Adaptive Finite Element Ocean Model. *Ocean Modelling* 56, 1–15. URL:
783 <http://www.sciencedirect.com/science/article/pii/S1463500312001023>, doi:10.1016/j.ocemod.2012.07.003.
- 784 Hirt, C.W., Nichols, B.D., 1981. Volume of Fluid (VOF) Method for the Dynamics of Free Boundaries. *Journal of Computational*
785 *Physics* 39, 201–225. URL: <http://www.sciencedirect.com/science/article/pii/0021999181901455>, doi:10.1016/0021-9991(81)90145-5.
- 786 Holmes, R., Long, D., Dodd, L.R., 1998. Large-Scale Debris and Submarine Landslides on the Barra Fan, west of
787 Britain. Geological Society, London, Special Publications 129, 67–79. URL: <http://sp.lyellcollection.org/content/129/1/67>,
788 doi:10.1144/GSL.SP.1998.129.01.05.
- 789 Horrillo, J., Wood, A., Kim, G.B., Parambath, A., 2013. A Simplified 3-D Navier-Stokes Numerical Model for Landslide-
790 Tsunami: Application to the Gulf of Mexico. *Journal of Geophysical Research: Oceans* 118, 6934–6950. URL:
791 <http://onlinelibrary.wiley.com/doi/10.1002/2012JC008689/abstract>, doi:10.1002/2012JC008689.
- 792 Hühnerbach, V., Masson, D.G., 2004. Landslides in the North Atlantic and its Adjacent Seas: An Analysis of Their Morphology,
793 Setting and Behaviour. *Marine Geology* 213, 343–362. URL: <http://www.sciencedirect.com/science/article/pii/S0025322704002774>,
794 doi:10.1016/j.margeo.2004.10.013.

- 795 IOC, I., 2008. BODC, 2008. Centenary Edition of the GEBCO Digital Atlas, published on CD-ROM on behalf of the Intergovernmental
796 Oceanographic Commission and the International Hydrographic Organization as part of the General Bathymetric Chart of the
797 Oceans. British oceanographic Data Centre, Liverpool .
- 798 Jiang, L., LeBlond, P., 1992. The Coupling of A Submarine Slide and The Surface Waves Which It Generates. *Journal of Geophysical*
799 *Research* 97, 12,731–12,744.
- 800 Jiang, L., LeBlond, P., 1993. Numerical Modeling of an Underwater Bingham Plastic Mudslide and the Waves Which it Generates.
801 *Journal of Geophysical Research* 98, 303–317. URL: <http://www.agu.org/pubs/crossref/1993/93JC00393.shtml>.
- 802 Kärnä, T., Kramer, S.C., Mitchell, L., Ham, D.A., Piggott, M.D., Baptista, A.M., 2018. Thetis coastal ocean model: discontin-
803 uous Galerkin discretization for the three-dimensional hydrostatic equations. *Geoscientific Model Development* 11, 4359–4382.
804 doi:10.5194/gmd-11-4359-2018.
- 805 Kirby, J.T., Shi, F., Nicolsky, D., Misra, S., 2016. The 27 April 1975 Kitimat, British Columbia, Submarine Landslide Tsunami:
806 A Comparison of Modeling Approaches. *Landslides* , 1–14 URL: <http://link.springer.com/article/10.1007/s10346-016-0682-x>,
807 doi:10.1007/s10346-016-0682-x.
- 808 Laberg, J., Vorren, T., Mienert, J., Bryn, P., Lien, R., 2002a. The Trænadjupet Slide: A Large Slope Fail-
809 ure Affecting the Continental Margin of Norway 4,000 Years Ago. *Geo-Marine Letters* 22, 19–24. URL:
810 <http://www.springerlink.com/content/dhy3y2nepbwa08b/abstract/>, doi:10.1007/s00367-002-0092-z.
- 811 Laberg, J., Vorren, T., Mienert, J., Evans, D., Lindberg, B., Ottesen, D., Kenyon, N., Henriksen, S., 2002b. Late Quater-
812 nary Palaeoenvironment and Chronology in the Trænadjupet Slide Area Offshore Norway. *Marine Geology* 188, 35–60. URL:
813 <http://www.sciencedirect.com/science/article/pii/S0025322702002748>, doi:10.1016/S0025-3227(02)00274-8.
- 814 Lee, C.H., Huang, Z., 2018. A two-phase flow model for submarine granular flows: With an application to collapse of deeply-submerged
815 granular columns. *Advances in water resources* 115, 286–300.
- 816 Løvholt, F., Harbitz, C.B., Haugen, K.B., 2005. A Parametric Study of Tsunami Generated by Submarine Slides
817 in the Ormen Lange/Storegga Area Off Western Norway. *Marine and Petroleum Geology* 22, 219–231. URL:
818 <http://linkinghub.elsevier.com/retrieve/pii/S0264817204001928>, doi:10.1016/j.marpetgeo.2004.10.017.
- 819 Løvholt, F., Pedersen, G., Harbitz, C.B., Glimsdal, S., Kim, J., 2015. On the Characteristics of Landslide Tsunamis. *Phil. Trans. R.*
820 *Soc. A* 373, 20140376. URL: <http://rsta.royalsocietypublishing.org/content/373/2053/20140376>, doi:10.1098/rsta.2014.0376.
- 821 Ma, G., Kirby, J.T., Shi, F., 2013. Numerical Simulation of Tsunami Waves Generated by Deformable Submarine Landslides. *Ocean*
822 *Modelling* 69, 146–165. URL: <http://www.sciencedirect.com/science/article/pii/S1463500313001170>, doi:10.1016/j.ocemod.2013.07.001.
- 823 Ma, G., Shi, F., Kirby, J.T., 2012. Shock-Capturing Non-Hydrostatic Model for Fully Dispersive Surface Wave Processes. *Ocean Mod-*
824 *elling* 43–44, 22–35. URL: <http://www.sciencedirect.com/science/article/pii/S1463500311001892>, doi:10.1016/j.ocemod.2011.12.002.
- 825 Masson, D.G., Harbitz, C.B., Wynn, R.B., Pedersen, G., Løvholt, F., 2006. Submarine Landslides: Processes, Triggers and Hazard
826 Prediction. *Philosophical Transactions of the Royal Society A: Mathematical, Physical and Engineering Sciences* 364, 2009–2039.
827 URL: <http://rsta.royalsocietypublishing.org/cgi/doi/10.1098/rsta.2006.1810>, doi:10.1098/rsta.2006.1810.
- 828 Mitchell, A.J., Allison, P.A., Piggott, M.D., Gorman, G.J., Pain, C.C., Hampson, G.J., 2010. Numerical Modelling of Tsunami Propa-
829 gation with Implications for Sedimentation in Ancient Epicontinental Seas: The Lower Jurassic Laurasian Seaway. *Sedimentology*
830 228, 81–97. URL: <http://www.sciencedirect.com/science/article/pii/S0037073810000692>.
- 831 Oishi, Y., Piggott, M.D., Maeda, T., Kramer, S.C., Collins, G.S., Tsuchida, H., Furumura, T., 2013. Three-Dimensional Tsunami
832 Propagation Simulations Using an Unstructured Mesh Finite Element Model. *Journal of Geophysical Research: Solid Earth* 118,
833 2998–3018. URL: <http://dx.doi.org/10.1002/jgrb.50225>, doi:10.1002/jgrb.50225.

- 834 Pan, W., Kramer, S.C., Kärnä, T., Piggott, M.D., 2020. Comparing non-hydrostatic extensions to a discontinuous finite element
835 coastal ocean model. *Ocean Modelling* , 101634doi:<https://doi.org/10.1016/j.ocemod.2020.101634>.
- 836 Pan, W., Kramer, S.C., Piggott, M.D., 2019. Multi-layer non-hydrostatic free surface modelling using the discontinuous galerkin
837 method. *Ocean Modelling* 134, 68–83.
- 838 Parkinson, S.D., Hill, J., Piggott, M.D., Allison, P.A., 2014. Direct Numerical Simulations of Particle-Laden Density Currents with
839 Adaptive, Discontinuous Finite Elements. *Geosci. Model Dev.* 7, 1945–1960. URL: <http://www.geosci-model-dev.net/7/1945/2014/>,
840 doi:10.5194/gmd-7-1945-2014.
- 841 Piggott, M.D., Gorman, G.J., Pain, C.C., Allison, P.A., Candy, A.S., Martin, B.T., Wells, M.R., 2008. A New Computational
842 Framework for Multi-Scale Ocean Modelling based on Adapting Unstructured Meshes. *International Journal for Numerical Methods*
843 *in Fluids* 56, 1003–1015. URL: <http://onlinelibrary.wiley.com/doi/10.1002/flid.1663/abstract>, doi:10.1002/flid.1663.
- 844 QGIS Development Team, 2009. QGIS Geographic Information System. Open Source Geospatial Foundation. URL:
845 <http://qgis.osgeo.org>.
- 846 Roberts, D., 1972. Slumping on the eastern margin of the Rockall Bank, North Atlantic Ocean. *Marine geology* 13, 225–237.
- 847 Salmanidou, D.M., Georgiopoulou, A., Guillas, S., Dias, F., others, 2015. Numerical Modelling of Mass Failure Processes and Tsunami-
848 genesis on the Rockall Trough, NE Atlantic Ocean, in: *The Twenty-fifth International Offshore and Polar Engineering Conference,*
849 *International Society of Offshore and Polar Engineers.* URL: <https://www.onepetro.org/conference-paper/ISOPE-I-15-479>.
- 850 Salmanidou, D.M., Guillas, S., Georgiopoulou, A., Dias, F., 2017. Statistical emulation of landslide-induced tsunamis
851 at the rockall bank, ne atlantic. *Proceedings of the Royal Society of London A: Mathematical, Physical and En-*
852 *gineering Sciences* 473. URL: <http://rspa.royalsocietypublishing.org/content/473/2200/20170026>, doi:10.1098/rspa.2017.0026,
853 arXiv:<http://rspa.royalsocietypublishing.org/content/473/2200/20170026.full.pdf>.
- 854 Shaw, B., Ambraseys, N.N., England, P.C., Floyd, M.A., Gorman, G.J., Higham, T.F.G., Jackson, J.A., Nocquet, J.M., Pain, C.C.,
855 Piggott, M.D., 2008. Eastern Mediterranean Tectonics and Tsunami Hazard Inferred from the AD 365 Earthquake. *Nature Geosci*
856 1, 268–276. URL: <http://dx.doi.org/10.1038/ngeo151>, doi:10.1038/ngeo151.
- 857 Smith, D., Shi, S., Cullingford, R., Dawson, A., Dawson, S., Firth, C., Foster, I., Fretwell, P., Haggart, B., Holloway, L., Long,
858 D., 2004. The Holocene Storegga Slide Tsunami in the United Kingdom. *Quaternary Science Reviews* 23, 2291–2321. URL:
859 <http://www.sciencedirect.com/science/article/pii/S0277379104001003>, doi:10.1016/j.quascirev.2004.04.001.
- 860 Smith, R.C., 2017. Numerical modelling of tsunami generated by deformable submarine slides. Ph.D. thesis.
- 861 Smith, R.C., Hill, J., Collins, G.S., Piggott, M.D., Kramer, S.C., Parkinson, S.D., Wilson, C., 2016. Comparing Approaches
862 for Numerical Modelling of Tsunami Generation by Deformable Submarine Slides. *Ocean Modelling* 100, 125–140. URL:
863 <http://www.sciencedirect.com/science/article/pii/S1463500316000354>, doi:10.1016/j.ocemod.2016.02.007.
- 864 Snelling, B.E., Collins, G.S., Piggott, M.D., Neethling, S.J., 2020. Improvements to a smooth particle hydrodynamics simulator for
865 investigating submarine landslide generated waves. *International Journal for Numerical Methods in Fluids* .
- 866 Solheim, A., Berg, K., Forsberg, C., Bryn, P., 2005. The Storegga Slide Complex: Repetitive Large Scale Sliding with Similar Cause
867 and Development. *Marine and Petroleum Geology* 22, 97–107. URL: <http://linkinghub.elsevier.com/retrieve/pii/S0264817204001813>,
868 doi:10.1016/j.marpetgeo.2004.10.013.
- 869 Talling, P., 2013. Waves on the Horizon. *Nature Geoscience* 3, 179–179. URL:
870 <http://www.nature.com/nclimate/journal/v3/n3/pdf/nclimate1815.pdf>.

- 871 Thomson, R.E., Rabinovich, A.B., Kulikov, E.A., Fine, I., Bornhold, B., 2001. On Numerical Simulation of the Landslide-Generated
872 Tsunami of November 3, 1994 in Skagway Harbor, Alaska, in: Hebenstreit, G. (Ed.), *Tsunami Research at the End of a Critical*
873 *Decade*. Springer Netherlands. volume 18 of *Advances in Natural and Technological Hazards Research*, pp. 243–282.
- 874 Tinti, S., Bortolucci, E., Chiavettieri, C., 2001. Tsunami Excitation by Submarine Slides in Shallow-water Approximation. *Pure and*
875 *Applied Geophysics* 158, 759–797. URL: <http://www.springerlink.com/index/10.1007/PL00001203>, doi:10.1007/PL00001203.
- 876 Wagner, B., Bennike, O., Klug, M., Cremer, H., 2007. First Indication of Storegga Tsunami Deposits from East Greenland. *Journal*
877 *of Quaternary Science* 22, 321–325. URL: <http://onlinelibrary.wiley.com/doi/10.1002/jqs.1064/abstract>, doi:10.1002/jqs.1064.
- 878 Ward, S.N., 2001. Landslide Tsunami. *Journal of Geophysical Research* 106, 11–201.
- 879 Watts, P., 1997. *Water Waves Generated by Underwater Landslides*. Ph.D. thesis. California Institute of Technology.
- 880 Watts, P., 1998. Wavemaker Curves for Tsunamis Generated by Underwater Landslides. *Journal of waterway, port, coastal, and ocean*
881 *engineering* 124, 127–137.
- 882 Watts, P., 2000. Tsunami Features of Solid Block Underwater Landslides. *Journal of Waterway, Port, Coastal, and Ocean Engineering*
883 126, 144–152. doi:10.1061/(ASCE)0733-950X(2000)126:3(144).
- 884 Watts, P., Grilli, S., Tappin, D., Fryer, G., 2005. Tsunami Generation by Submarine Mass Failure. II: Predic-
885 tive Equations and Case Studies. *Journal of Waterway, Port, Coastal, and Ocean Engineering* , 298–310URL:
886 [http://ascelibrary.org/doi/abs/10.1061/\(ASCE\)0733-950X\(2005\)131:6\(298\)](http://ascelibrary.org/doi/abs/10.1061/(ASCE)0733-950X(2005)131:6(298)).
- 887 Watts, P., Grilli, S.T., Kirby, J.T., Fryer, G.J., Tappin, D.R., 2003. Landslide Tsunami Case Studies Using a Boussinesq
888 Model and a Fully Nonlinear Tsunami Generation Model. *Natural Hazards and Earth System Science* 3, 391–402. URL:
889 <http://www.nat-hazards-earth-syst-sci.net/3/391/2003/>, doi:10.5194/nhess-3-391-2003.
- 890 Watts, P., Imamura, F., Grilli, S., 2000. Comparing Model Simulations of Three Benchmark Tsunami Generation Cases. *Science of*
891 *Tsunami Hazards* , 1–17.
- 892 Wells, M.R., Allison, P.A., Hampson, G.J., Piggott, M.D., Pain, C.C., 2005. Modelling Ancient Tides: the
893 Upper Carboniferous Epi-Continental Seaway of Northwest Europe. *Sedimentology* 52, 715–735. URL:
894 <http://onlinelibrary.wiley.com/doi/10.1111/j.1365-3091.2005.00718.x/abstract>, doi:10.1111/j.1365-3091.2005.00718.x.
- 895 Wells, M.R., Allison, P.A., Piggott, M.D., Hampson, G.J., Pain, C.C., Gorman, G.J., 2010. Tidal Modeling of an Ancient Tide-
896 Dominated Seaway, Part 1: Model Validation and Application to Global Early Cretaceous (Aptian) Tides. *Journal of Sedimentary*
897 *Research* 80, 393–410. URL: <http://jsedres.geoscienceworld.org/content/80/5/393>, doi:10.2110/jsr.2010.044.
- 898 Wiegel, R.L., 1955. Laboratory Studies of Gravity Waves Generated by the Movement of a Submarine Body. *Transactions of the*
899 *American Geophysical Union* 36, 759–774.
- 900 Yavari-Ramshe, S., Ataie-Ashtiani, B., 2015. A Rigorous Finite Volume Model to Simulate Subaerial and Submarine Landslide-
901 Generated Waves. *Landslides* , 1–19URL: <http://link.springer.com/article/10.1007/s10346-015-0662-6>, doi:10.1007/s10346-015-0662-
902 6.
- 903 Yu, M.L., Lee, C.H., 2019. Multi-phase-flow modeling of underwater landslides on an inclined plane and consequently generated waves.
904 *Advances in Water Resources* 133, 103421.

905 **8. Supplementary Data**

906 Example set-up files for the different approaches within Fluidity for each scenario
907 can be found on the following link: <https://dx.doi.org/10.6084/m9.figshare.3507734>

Approach	Scenario	Dimenions	Filename
MM2FS	Gulf of Mexico	2D	gom_2mat.flml
SM-DS-SV	Gulf of Mexico	2D	gom_SMDSSV_2D.flml
SM-RS-SV	Gulf of Mexico	2D	gom_SMRSSV_2D.flml
SM-RS-EV	Gulf of Mexico	2D	gom_SMRSEV_2D.flml
SM-DS-SV	R1 - Rockall Bank	3D	rockall_SMDSSV.flml
SM-RS-SV	R2- Rockall Bank	3D	rockall_SMRSSV.flml
SM-RS-EV	R3- Rockall Bank	3D	rockall_SMRSEV.flml

908 **extract slide shape.py** can be used to extract the slide thickness from the
909 output of an MM2FS simulation.

910 **9. Figures**

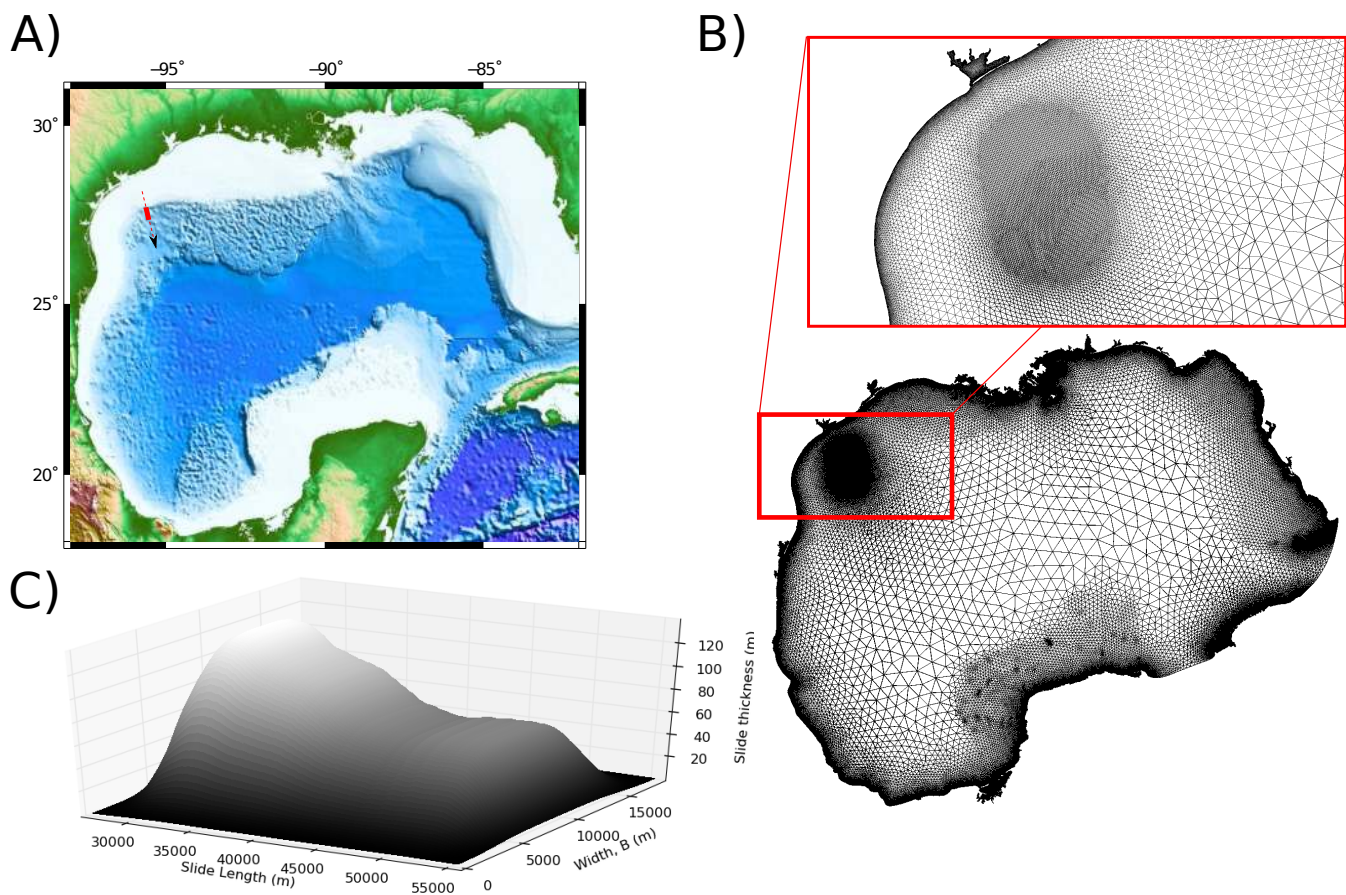


Figure 1: Model setup for the Gulf of Mexico verification test. A) Map of the Gulf of Mexico, including location of slide (rectangle) and direction of slide motion (dashed arrow). B) Overview of the mesh (bottom) with enlargement of the mesh in the region of the slide showing the increased resolution. C) Three-dimensional shape of the slide used in the simulations.

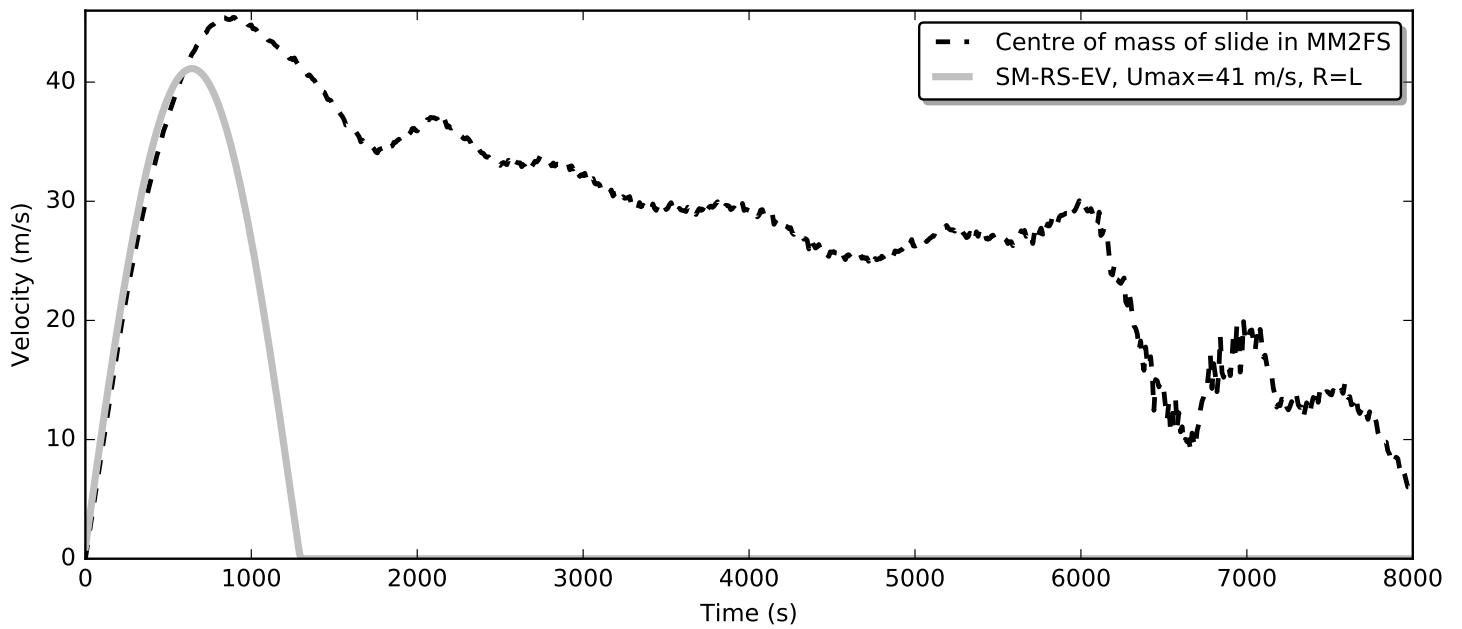
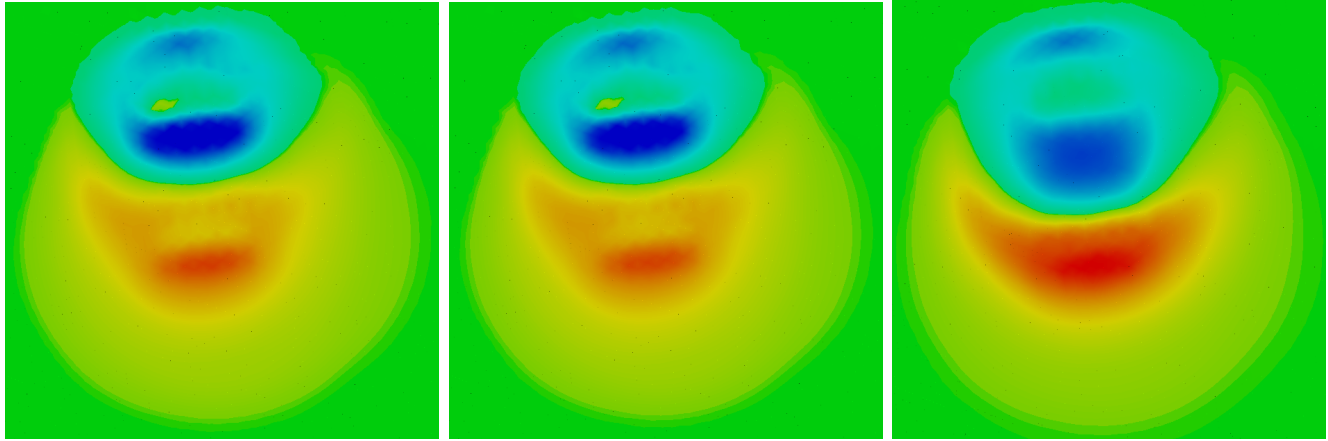
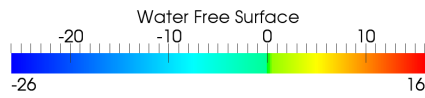


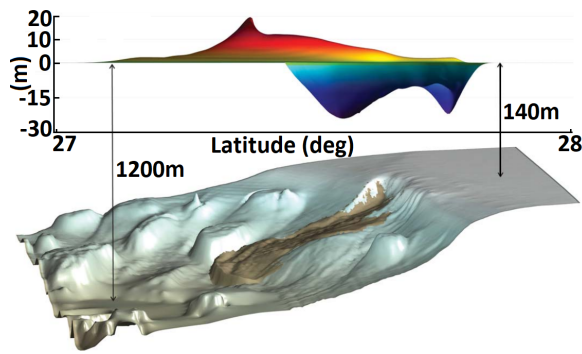
Figure 2: Comparison of velocity profiles for the SM-RS-EV approach (for the velocity of the slide’s centre of mass in the MM2FS approach, dashed line), and for the SM-RS-SV approach with maximum velocity 41m/s (grey line). Although the velocity profiles are not similar after the first 1000s, the acceleration of the slides in the early part of slide movement are well matched, and it is this initial acceleration that is important for wave generation.



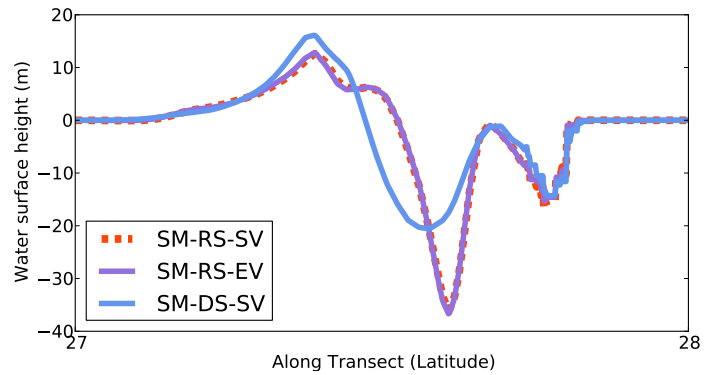
(a) SM-RS-EV, 7 mins

(b) SM-RS-SV, 7 mins

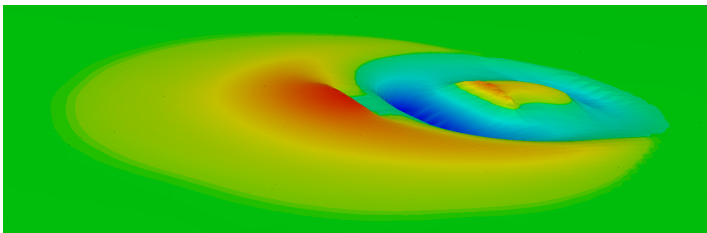
(c) SM-DS-SV, 7 mins



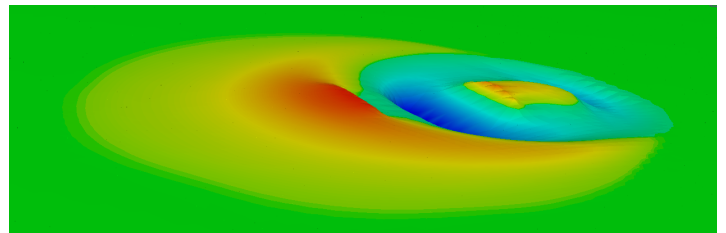
(d) TSUNAMI3D, 7 mins



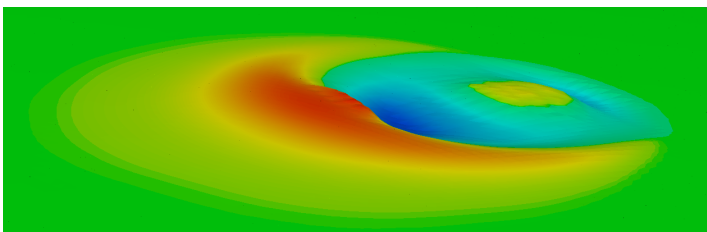
(e) Water elevation along transect through middle of the slide



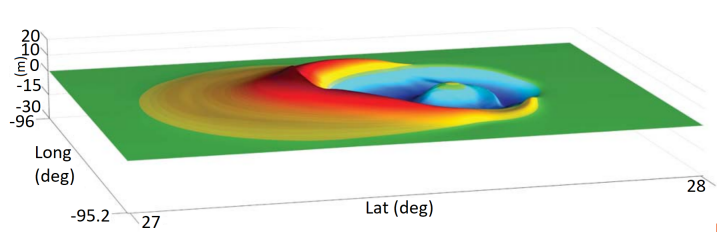
(f) SM-RS-EV, 10 mins



(g) SM-RS-SV, 10 mins



(h) SM-DS-SV, 10 mins



(i) TSUNAMI3D, 10 mins

Figure 3: Wave heights 7 minutes after slide initiation for (a) SM-RS-EV (b) SM-RS-SV (c) SM-DS-SV in the Gulf of Mexico test case. (d) shows results from Horrillo et al. (2013) for comparison. (e) shows the water elevation across the transect shown in Figure 1, this is the midpoint of the width of the slide. Colour plots shown span 27° – 28° N and 95.2° – 96° W.

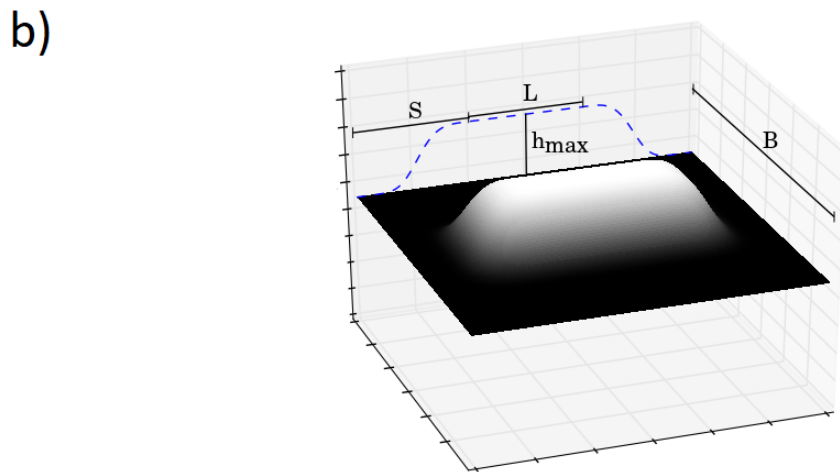
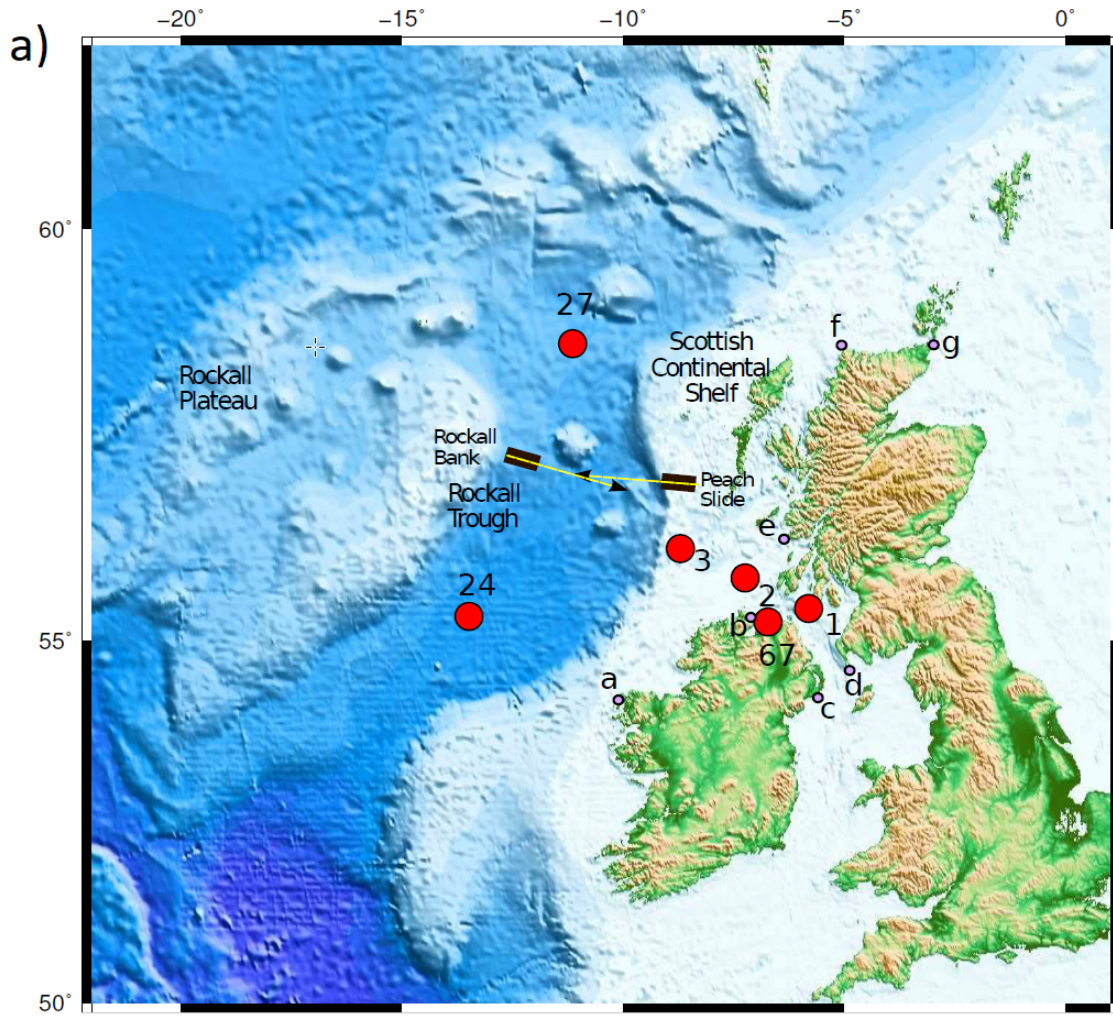


Figure 4: A) Map of British Isles with locations of Rockall Bank and Peach Slides, with arrows indicating directions of failure. Important bathymetric features are labelled. Red dots show locations of some of the numerical wave gauges to be considered later. B) Shape of rigid slide (exaggerated vertically) used in three dimensions, as described by Equation 11.

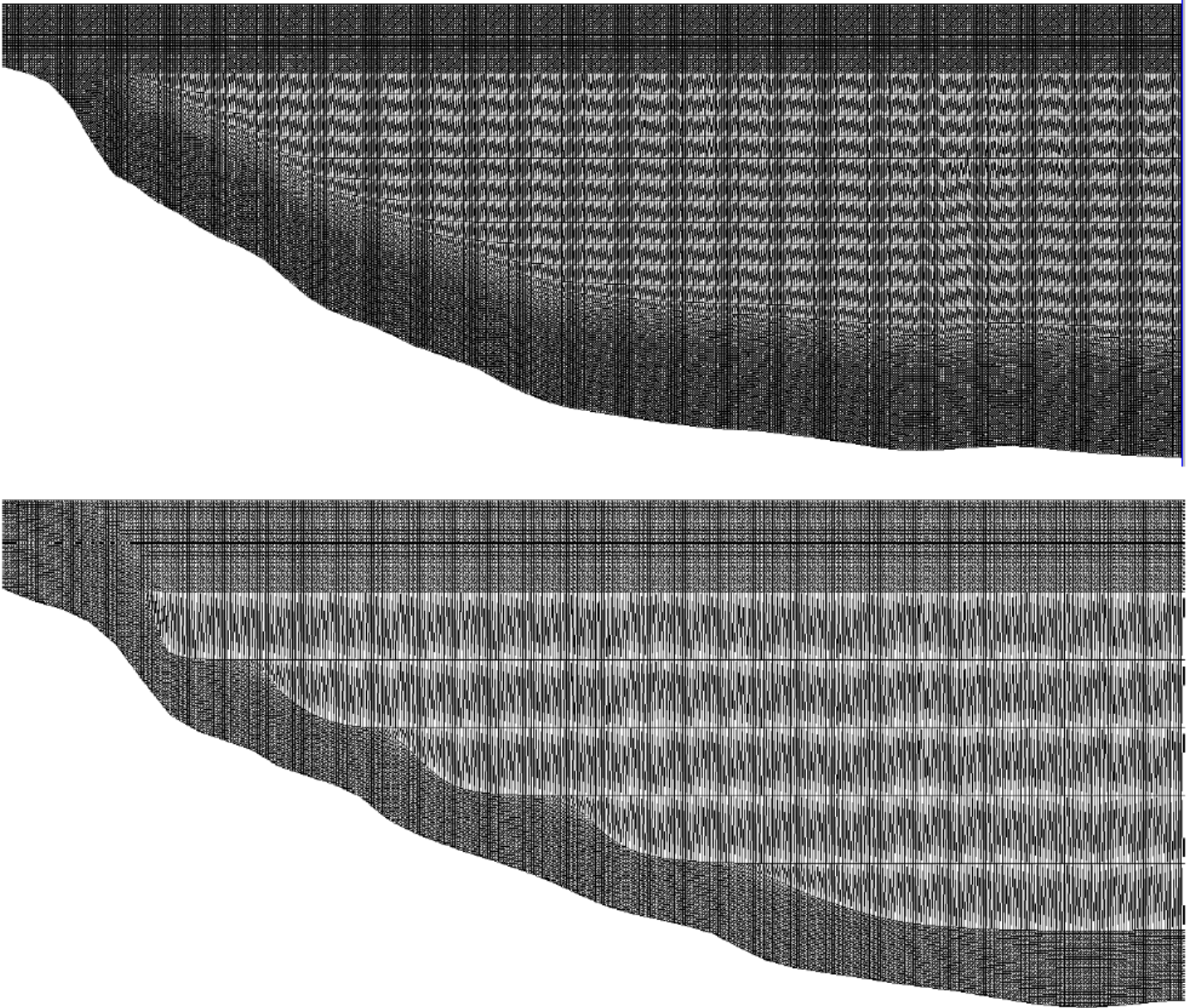
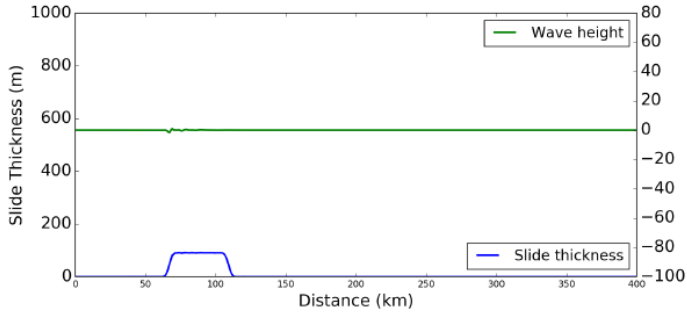
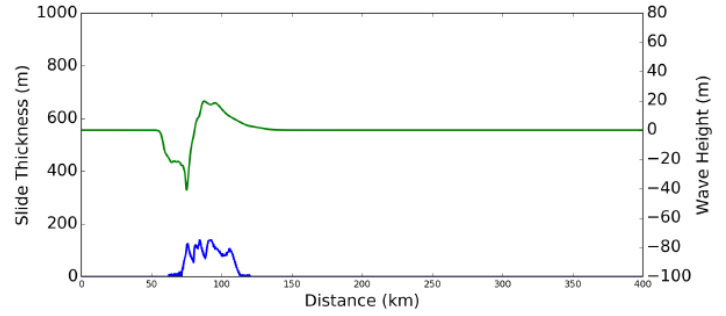


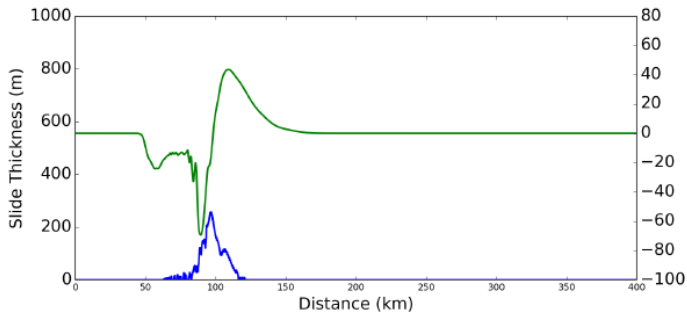
Figure 5: Section of Rockall Mesh (top) containing 2653 nodes and Peach Slide Mesh (bottom) containing 2984 nodes. There is a vertical exaggeration of $\times 10$



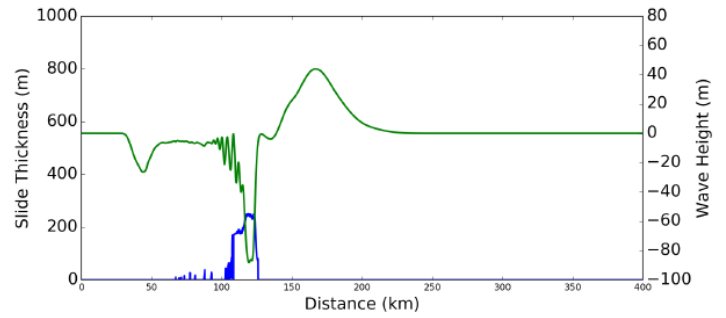
(a) 10 seconds



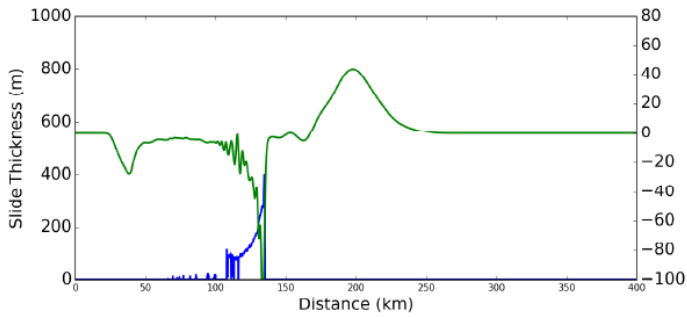
(b) 200 seconds



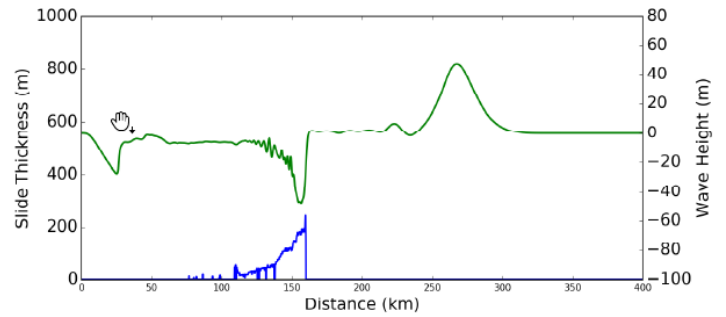
(c) 400 seconds



(d) 800 seconds

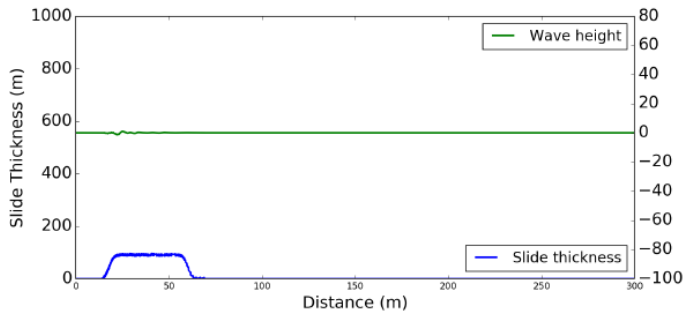


(e) 1000 seconds

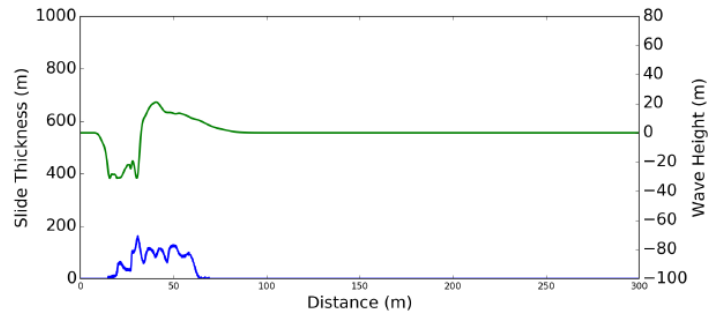


(f) 1500 seconds

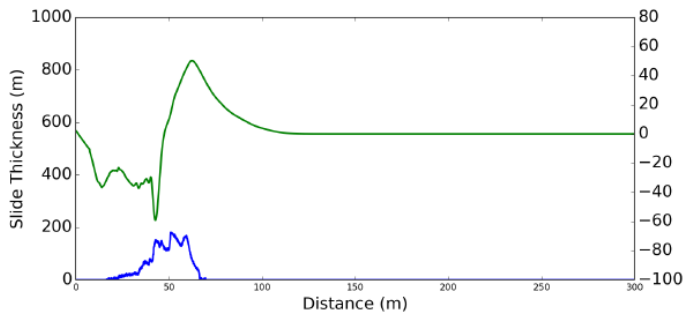
Figure 6: Slide thickness (blue) and wave height (green) for two-dimensional submarine slide at Rockall Bank, extracted from MM2FS simulation. Both are vertically exaggerated on different scales.



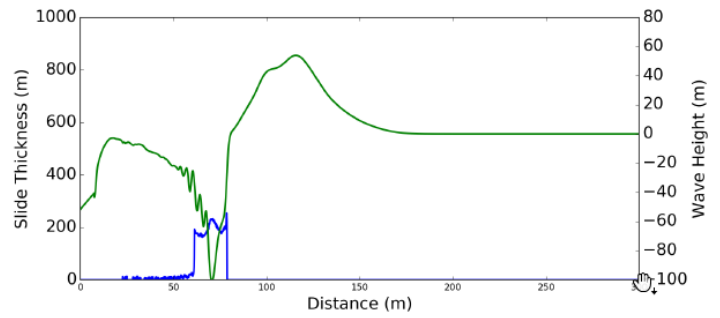
(a) 10 seconds



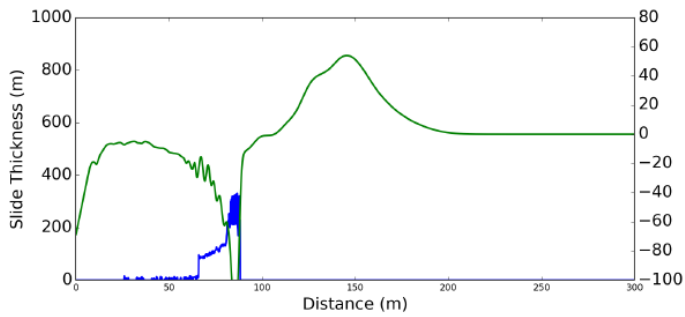
(b) 200 seconds



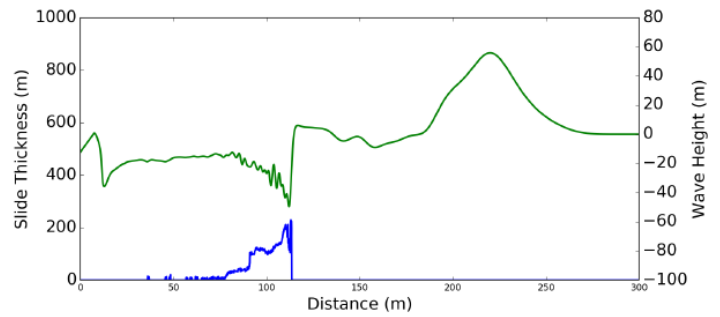
(c) 400 seconds



(d) 800 seconds



(e) 1000 seconds



(f) 1500 seconds

Figure 7: Slide thickness (blue) and wave height (green) for two-dimensional submarine slide at Peach Slide, extracted from MM2FS simulation. Both are vertically exaggerated on different scales.

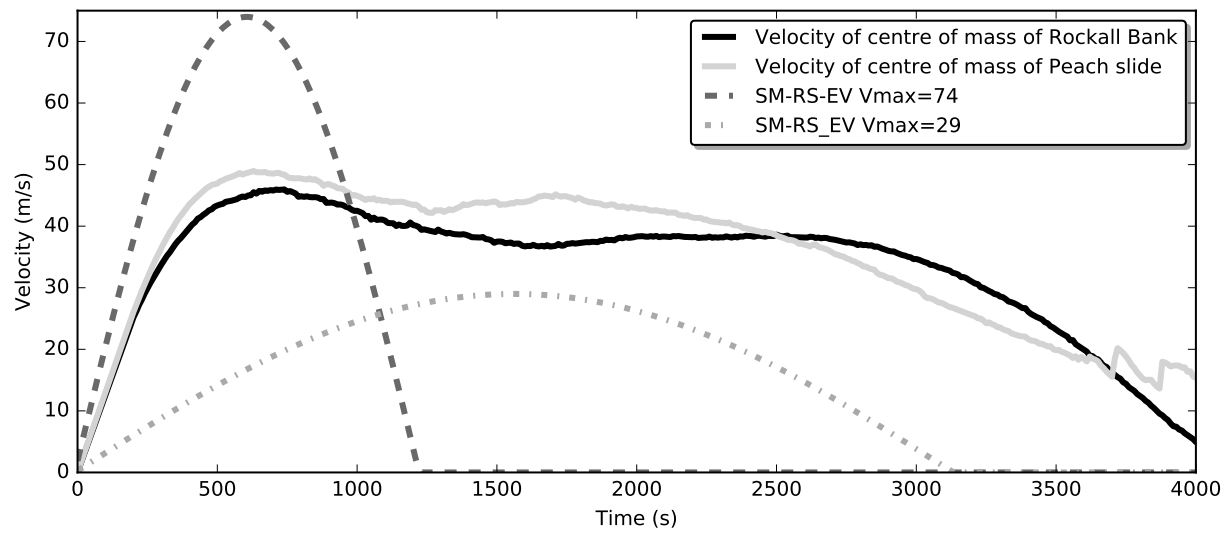


Figure 8: Velocity profiles representing the movement of the slide's centre of mass for Rockall Bank (solid black) and Peach slides (solid grey) and estimated slide velocity profiles for Rockall Bank scenarios with maximum velocities of 74m/s (dark grey, dashed) and 29 m/s (light grey, dot-dashed).

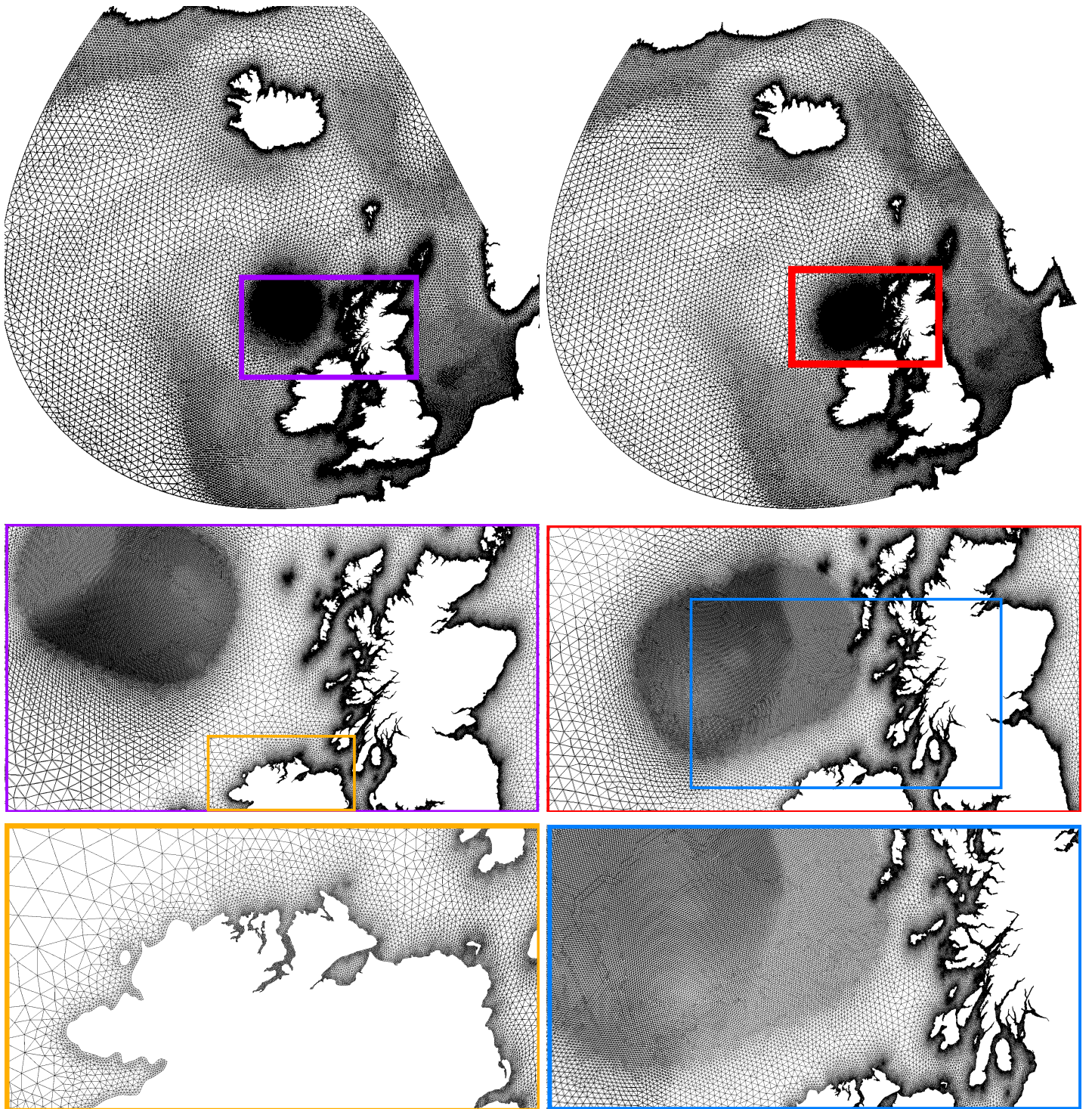
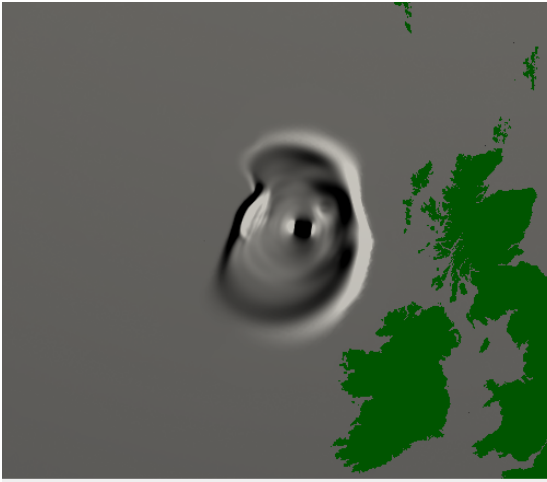
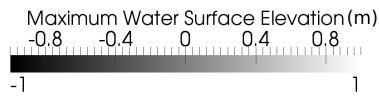
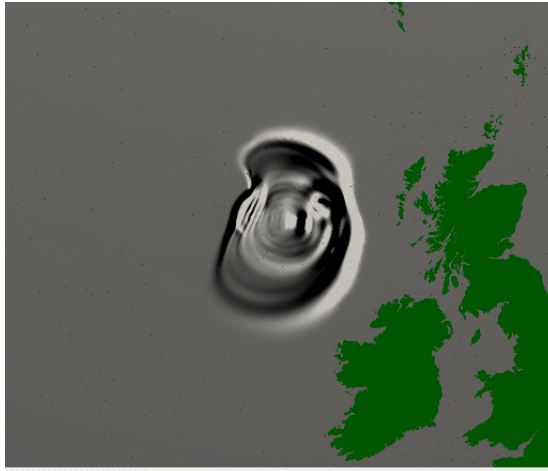


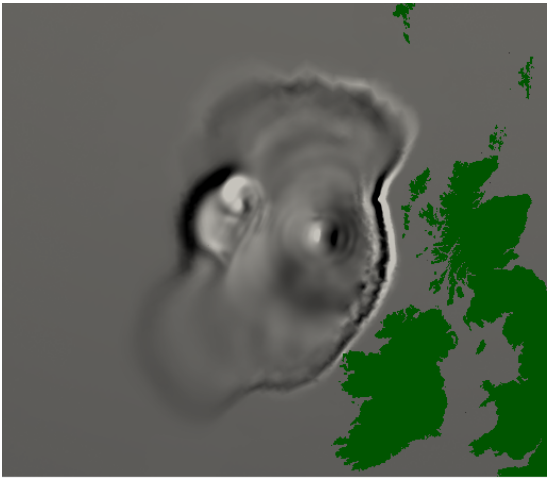
Figure 9: Left: Mesh for Rockall Bank simulations containing 151892 nodes. Right: Mesh for Peach Slide simulations containing 150257 nodes. The minimum edge length is 0.5 km and the maximum edge length is 50 km. The three dimensional domains have maximum extents at approximately 49°N, 70°N, 13°E, 30°W.



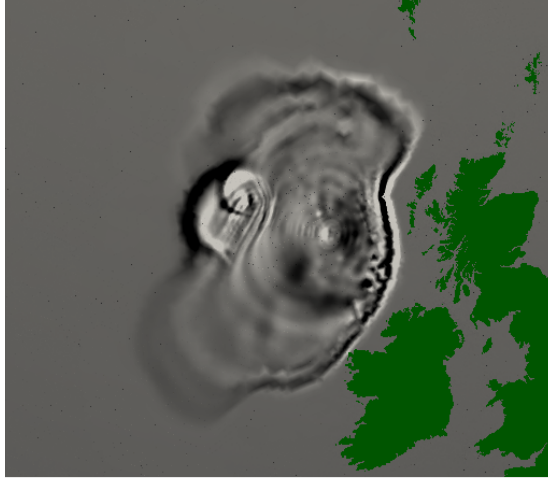
(a) SM-RS-SV, 30 mins



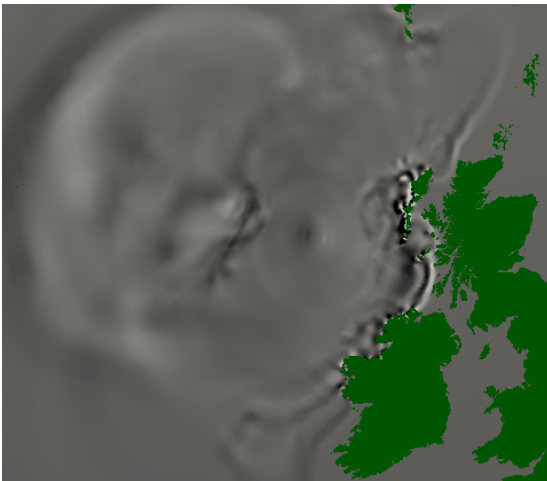
(b) SM-DS-SV, 30 mins



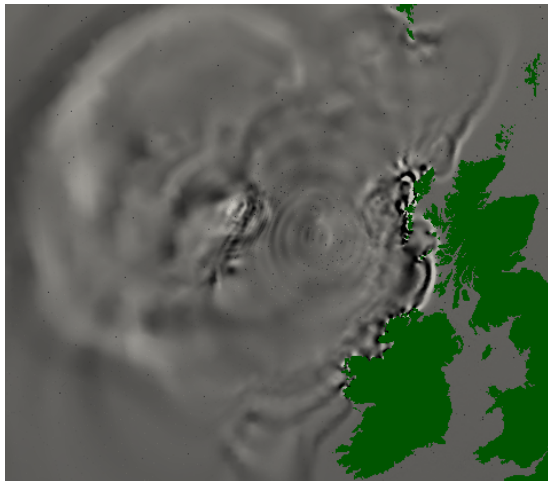
(c) SM-RS-SV, 60 mins



(d) SM-DS-SV, 60 mins

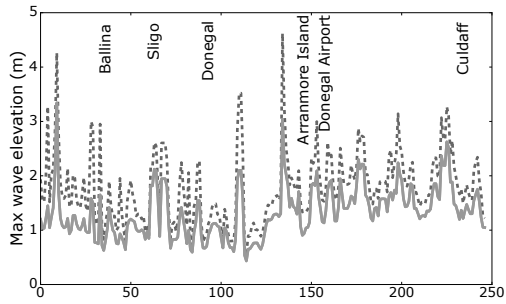


(e) SM-RS-SV, 110 mins

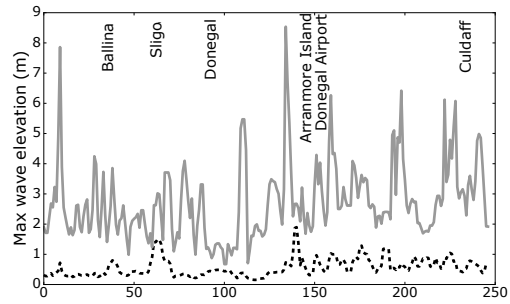


(f) SM-DS-SV, 120 mins

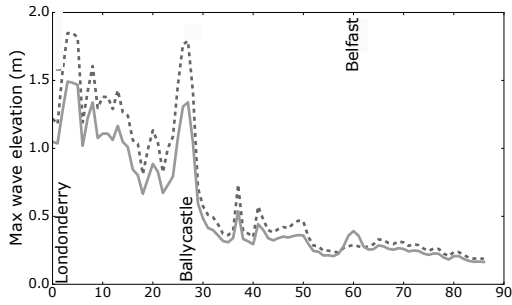
Figure 10: Wave height through time for Rockall Bank slide for the SM-RS-SV approach (left) and the SM-DS-SV approach (right). The scales for wave amplitude is capped at ± 1 m.



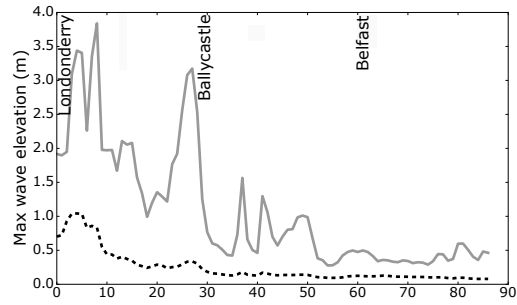
(a) West Ireland (a to b)



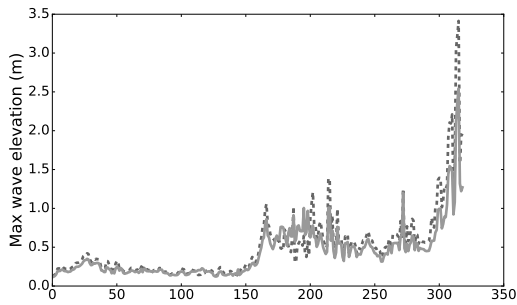
(b) West Ireland (a to b)



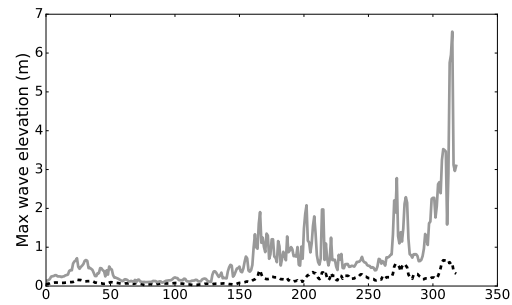
(c) Northern Ireland (b to c)



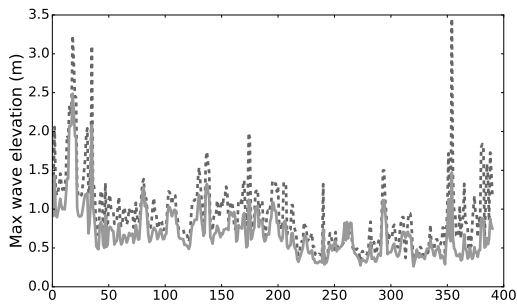
(d) Northern Ireland (b to c)



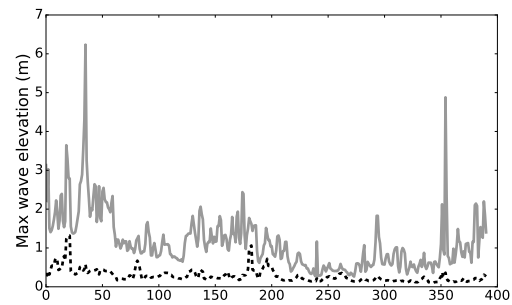
(e) South West Scotland (d to e)



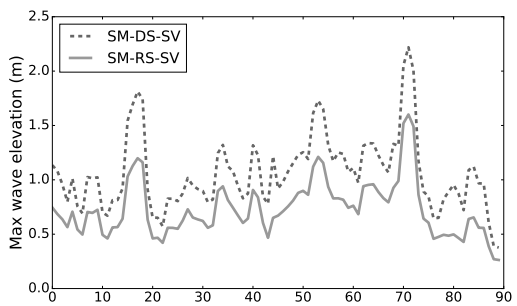
(f) South West Scotland (d to e)



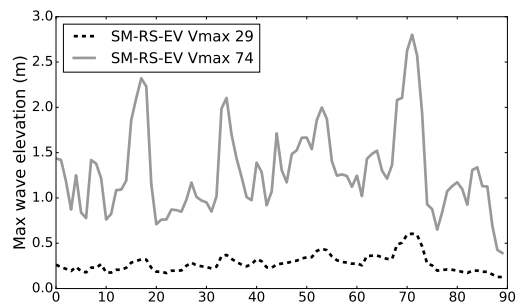
(g) North West Scotland (e to f)



(h) North West Scotland (e to f)

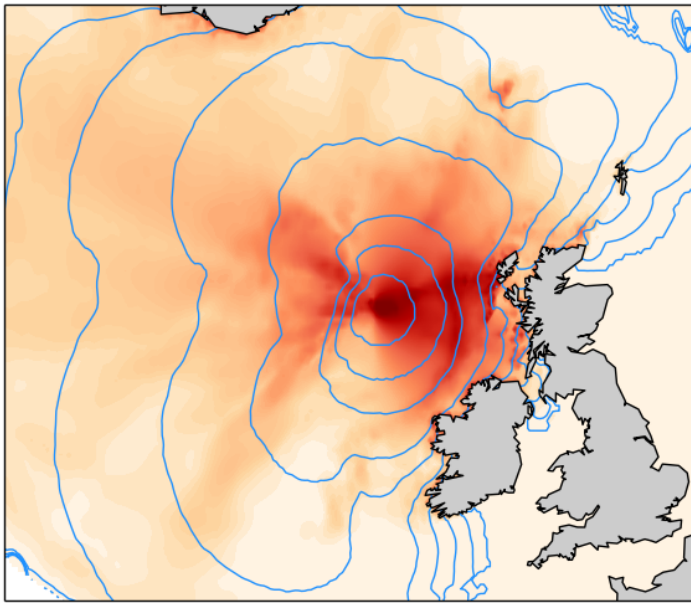


(i) North Scotland (f to g)

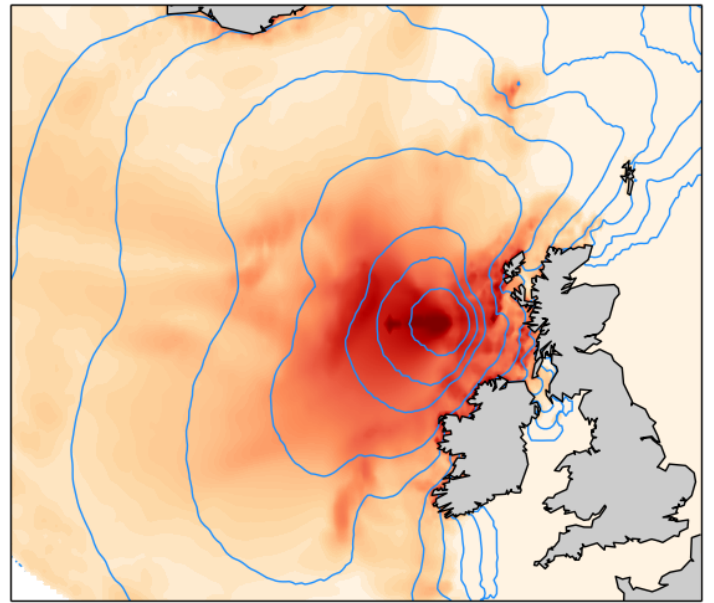


(j) North Scotland (f to g)

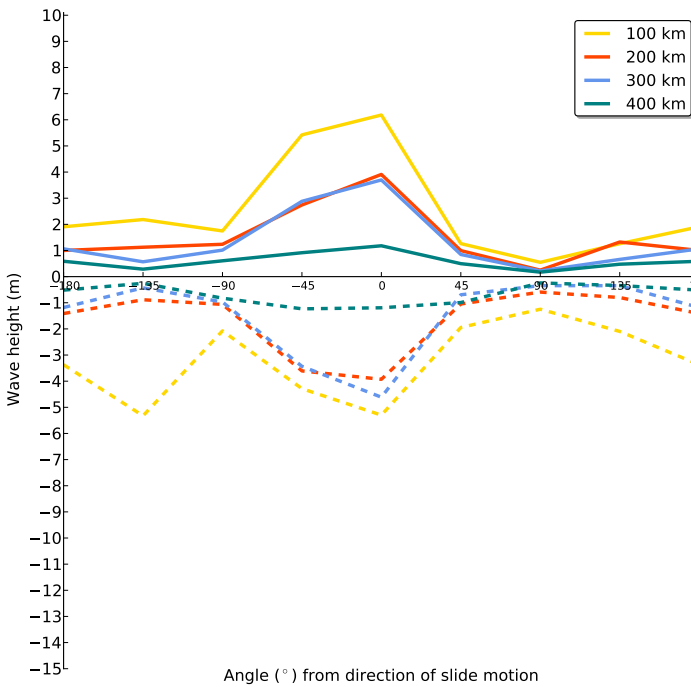
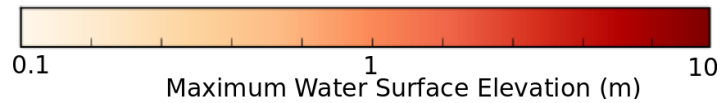
Figure 11: Maximum water elevation at sections of coastline shown in Figure 4 for R1 vs R2 (left) and R3 vs R4 (right).



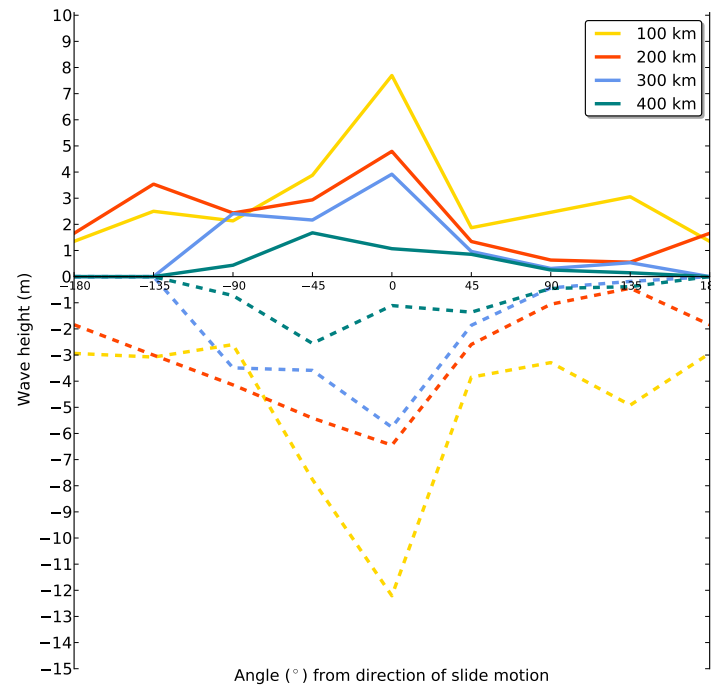
(a) Rockall Bank (SM-DS-SV)



(b) Peach slide (SM-DS-SV)



(c) Rockall Bank (SM-DS-SV)



(d) Peach slide (SM-DS-SV)

Figure 12: Top: Maximum Water Elevation in first 4 hours and 15 mins after slide initiation for Rockall Bank Slide (left) and Peach slide (right) using SM-DS-SV approaches. Bottom: Maximum (solid lines) and minimum (dashed lines) wave heights recorded at numerical wave gauges 100 km (yellow), 200 km (red), 300 km (blue) and 400 km (green) from Rockall Bank (left) and Peach Slide (right) for SM-DS-SV.